Microscopic dynamics of molecular liquids and glasses: Role of orientations and translation-rotation coupling

T. Theenhaus, R. Schilling, A. Latz,* and M. Letz†
Institut für Physik, Johannes Gutenberg-Universität, Staudinger Weg 7, D-55099 Mainz, Germany
(Received 21 May 2001; published 22 October 2001)

We investigate the dynamics of a fluid of dipolar hard spheres in its liquid and glassy phases, with emphasis on the microscopic time or frequency regime. This system shows rather different glass transition scenarios related to its rich equilibrium behavior, which ranges from a simple hard sphere fluid to long range ferroelectric orientational order. In the liquid phase close to the ideal glass transition line and in the glassy regime a medium range orientational order occurs leading to a softening of an orientational mode. To investigate the role of this mode we use the molecular mode-coupling equations to calculate the spectra $\phi''_{lm}(q,\omega)$ and $\chi''_{lm}(q,\omega)$. In the center of mass spectra $\phi''_{00}(q,\omega)$ and $\chi''_{00}(q,\omega)$ we found, besides a high frequency peak at ω_{hf}, a peak at ω_{op}, about one decade below ω_{hf}. ω_{op} has almost no q dependence and exhibits an ''isotope'' effect $\omega_{op}\propto I^{-1/2}$, with I the moment of inertia. We give evidence that the existence of this peak is related to the occurrence of medium range orientational order. It is shown that some of these features also exist for schematic mode coupling models.

DOI: 10.1103/PhysRevE.64.051505 PACS number(s): 64.70.Pf, 61.25.Em, 61.20.Lc

I. INTRODUCTION

The dynamical properties of liquids and glasses are still a challenging problem. In the vicinity of the glass transition the frequency (or time) range can be decomposed into at least three different domains, the α, β, and microscopic regimes. The first one describes the structural relaxation, which dramatically slows down when the glass transition is approached from above. In the idealized mode-coupling theory (MCT) for simple liquids [1–4] and for molecular systems [5–7] it even stops at a critical temperature T_c. Probably the most interesting result of MCT is the existence of the so-called β relaxation, which describes the dynamics within a cage of particles above and below T_c. The corresponding β frequency scale is much larger than that for α relaxation. At still higher frequencies there are vibrational and librational motions, which constitute the microscopic regime.

One may say that most of the attention in the field of glassy dynamics during the last 15 years has been devoted to α and β relaxation. This activity has been mainly stimulated by MCT which in these two regimes predicted scaling laws with diverging α and β time scales. These predictions have been tested intensively by experiments and numerical simulations. A satisfactory agreement has been found for many glass forming systems [7–15]. Experimental and simulation results do not exhibit any singular or crossover behavior for microscopic frequencies ω, i.e., for $\omega \geqslant 1$ THz. Nevertheless, in that regime an interesting phenomenon occurs in most glasses but not in crystals and colloidal glasses, the so-called boson peak. Indications for this peak came from two different sides. First, the low temperature specific heat $c(T)/c_D(T)$ scaled by the phonon contribution $c_D(T)\propto T^3$ shows a peak at about 10 K for several glass formers (see, e.g., [16]). This excess with respect to $c_D(T)$ around 10 K implies the existence of additional excitations besides the long wavelength acoustic phonons. Second, Raman spectra $I(\omega)$ compared to the phonon contribution $I_D(\omega)\propto\omega^2$ exhibit at about 1 THz an excess also (see, e.g., [17]). Since the temperature dependence of the excess intensity scales with the Bose distribution function $n_B(T)$, the peak is called the boson peak.

That these two observations might have a common origin was first shown by Buchenau *et al.* [18,19]. For vitreous silica these authors also found an excess with respect to $g_D(\omega)\propto\omega^2$ for the vibrational density of states $g(\omega)$ determined from inelastic neutron scattering (INS) data. Using $g(\omega)$ to calculate $c(T)/c_D(T)$ led to good agreement with the result from heat capacity measurements. In particular, the peak positions for both results coincided. Although the boson peak does not seem to posses any singular ω or T dependence it is a universal phenomenon for all systems with the exception of glass forming colloids, in the sense that it appears more or less for almost all glass formers. For, e.g., LiCl solutions [11] and orthoterphenyl [20], it has been stressed that the boson peak, together with the narrowing of a central peak at $\omega=0$, develops continuously from the liquid to the glassy phase.

Despite considerable experimental and numerical effort its microscopic origin is still not satisfactorily understood. Two reasons might be responsible for that. First, e.g., in the case of light scattering, the precise connection between the measured quantity and the basic theoretical objects, the time- or frequency-dependent site-site or molecular correlation functions for molecular liquids, is not known. For instance, it has been shown that several coupling mechanisms between light and distinct modes of liquid $ZnCl_2$ exist which have different ω-dependent coupling constants [21]. This may

*Present address: Institut für Physik, Reichenhainer Strasse 70, TU-Chemnitz, D-09107 Chemnitz, Germany.
†Present address: Schott Glas, Research and Developement, Hattenbergstrasse 10, 55014 Mainz, Germany.

complicate the determination of $g(\omega)$ from Raman spectra. Second, the relationship between the various t- or ω-dependent correlators and microscopic modes obtained from a diagonalization of the dynamical matrix is not obvious. In addition, these correlators can be calculated analytically only under serious approximations. It is apparent that numerical investigations represent a powerful tool since their microscopic nature allows calculation of both the correlators or spectra and under certain conditions the microscopic modes. The possible character of these modes ranges as follows.

vibrational	$\leftrightarrow$	relaxational
extended	$\leftrightarrow$	localized
propagating	$\leftrightarrow$	non-propagating
harmonic	$\leftrightarrow$	anharmonic
longitudinal	$\leftrightarrow$	transversal
coherent	$\leftrightarrow$	random
translational	$\leftrightarrow$	rotational
acoustic	$\leftrightarrow$	optic

Since these feature can occur in combinations, the complexity of the problem becomes obvious. In addition, different experimental approaches to a specific material or a specific measurement of different types of glass former, e.g., strong or fragile ones, may exhibit different features of the same phenomenon.

Without demanding completeness let us briefly review the present status. Inelastic x-ray scattering (IXS) on v-SiO_2 gave evidence that propagating acoustic sound waves exist even above ω_{BP}, the position of the boson peak [22]. This led these authors to conclude that the propagating modes are also involved in the boson-peak itself. On the other hand, a crossover at ω_{BP} from propagating to localized (strongly scattered) acoustic modes was deduced for v-SiO_2 from INS and IXS [23]. Comments on this controversy are given in Refs. [24–26]. However, interpretations of IXS experiments that are free of any model have recently strengthened at least the fact that there are propagating modes above ω_{BP} [27,28]. Molecular dynamics (MD) simulations for v-SiO_2 have given evidence that the boson-peak modes cannot be strongly localized and that there is a contribution of transverse propagating modes in the boson-peak regime [29,30]. IXS experiments for LiCl solutions and glycerol seem to detect propagating *longitudinal* modes at ω_{BP} [31], whereas a MD simulation for H_2O shows a mixing of propagating longitudinal and transverse modes, at least for large enough q ($q>4$ nm^{-1}) [32].

Further important information about the nature of the boson-peak modes comes from a normal mode analysis for a system of soft spheres [33] and for SiO_2 deep in its glass phase [34–37]. There was found that these modes are harmonic and quasi localized [33,36]. They occur due to hybridization of localized low frequency optic modes with propagating acoustic states [34] and are extended but nonpropagating. In addition each normal mode has a coherent and a random component. The latter finding is consistent with other numerical results for a Lennard-Jones liquid [38] and liquid $ZnCl_2$ [21,39,40], and conclusions drawn from experimental data for various glass formers [41,42]. Since $ZnCl_2$ was considered in its liquid phase, only an instantaneous normal mode analysis is feasible. Restriction to the stable modes accurately reproduces in the microscopic frequency regime the dynamical structure factor $S(q,\omega)$ obtained from a MD simulation [40]. This implies a harmonic mode character at temperatures even above the MCT glass transition temperature T_c.

There is not much analytical work on the boson peak. For a harmonic crystal with random spring constants it has been shown [43,44] that an excess density of states follows. It has recently been stressed [45] that the approach in [44] has some shortcomings which may be removed by use of off-lattice models [46]. Another theoretical framework is the soft potential model [47–50] which allows a description of the low temperature anomalies below 1 K and those at 10–20 K, that includes the excess density of states.

As already mentioned above, MCT has been rather successful in describing the α and β dynamics. Schematic MCT models [1] where the wave number dependence was neglected were also used to describe experimental spectra in the microscopic regime, including the boson peak [11,51–56]. Whereas the results in Fig. 6 of Ref. [11] and Fig. 4 of Ref. [53] yield spectra that are reminiscent of boson-peak spectra the line shape does not come out satisfactorily. However, recently a detailed MCT investigation for a glass of hard spheres was performed, including the q dependence [57]. Besides a high frequency peak at ω_{hf} an additional peak at ω_{AOP}, about one decade below ω_{hf}, was seen for a volume fraction $\varphi=0.6$. This peak, which strongly resembles that in Refs. [11] (Fig. 6) and [52] (Fig. 7), originates from the distribution of harmonic oscillators within the cages and has been called the *anomalous oscillation peak* (AOP). As explicitly demonstrated [57], it shares many features with the boson peak.

In contrast to a system of hard spheres or binary van der Waals liquids, molecular liquids also have orientational degrees of freedom. One may ask: Does the boson peak also involve orientational motion? Indeed, one of its first interpretations for v-SiO_2 involved coupled rotations of SiO_4 tetrahedra [18]. Such an interpretation was supported by MD simulations for v-SiO_2 [35,58] and $ZnCl_2$ [40] and by neutron scattering experiments, proving nonsoundlike contributions around ω_{BP} [59]. Dielectric loss measurements probe the orientational dynamics only. Since these measurements, e.g., for glycerol and propylene carbonate, also exhibit a boson peak [60,61], this gives additional evidence that this peak may also be related to the orientational degrees of freedom. The role of orientational modes becomes even clearer from experiments on ethanol [62,63]. Around 100 K, ethanol can occur in several phases: a glass phase, an orientational glass phase, a crystalline phase and a rotator phase. The center of mass positions of the molecules are frozen in an amorphous structure for the glass phase, and in a crystalline structure for the three other phases. The orientational dynamic is nonergodic for the glass and the orientational glass and ergodic for the crystal and the rotator phase. INS has shown the existence of a boson peak for the orientational glass which does not differ much from that in the glass. Even in the rotator phase there is a boson peak, but it is shifted to

lower frequencies. Similarly to structural glasses the orientational glass phase also exhibits an excess in the specific heat $c(T)/c_D(T)$ [62]. These findings suggest that these excess modes are primarily related to the orientational degrees of freedom.

In the present paper we will not calculate the density of states, but the susceptibility and correlation spectra of the collective dynamics. These quantities show the appearance of an extra peak about a decade below the high frequency peak, where the former also originates from the orientational degrees of motion.

The outline of the paper is as follows. In Sec. II, we will briefly review the derivation of the equation of motion for the relevant correlators of rigid, linear molecules and the mode-coupling approximation. In addition, we will discuss the linearized equations. The molecular mode-coupling equations are solved numerically for a liquid of dipolar hard spheres in Sec. II D. Finally, Sec. III contains a discussion of the results and some conclusions.

II. MOLECULAR DYNAMICS

In the first part of this section we will present the equations of motion for the most relevant correlation functions of a molecular liquid. The second part contains a discussion of the corresponding linearized equations, which yields information on the microscopic time scale, and in the third part we will briefly review the mode-coupling approximation.

A. Equation of motion

We restrict ourselves to a system of N rigid and linear molecules with mass M and moment of inertia I. There are two possibilities to describe molecular liquids: a *site-site* or a *molecular* representation [64]. The latter, which will be chosen here, decomposes the $5N$ degrees of freedom into $3N$ translational and $2N$ orientational ones. Of particular interest are the molecular correlators $\mathbf{S}(\vec{q},t)=(S_{lm,l'm'}(\vec{q},t))$ [5,6]. The partial dynamical structure factors in a site-site description are linear superpositions of $S_{lm,l'm'}(\vec{q},t)$ but not vice versa [65].

The Mori-Zwanzig formalism has been used to derive equations of motion for $\mathbf{S}(\vec{q},t)$ for a single linear molecule in a liquid of isotropic particles [5] and for a molecular liquid of linear [6] and arbitrary molecules [7]. Similar work has been done in a site-site description [66]. A comparison between the tensorial and the site-site mode-coupling theories has recently been performed for a single dumbbell in a liquid of hard spheres [67].

It turns out that the original form of the equations of motion is not suitable for a numerical solution. Therefore we have rewritten those equations as follows:

$$\dot{\mathbf{S}}(\vec{q},t)+i\sum_{\alpha}\mathbf{q}^{\alpha}\mathbf{S}^{\alpha}(\vec{q},t)=0, \tag{1a}$$

$$\dot{\mathbf{S}}^{\alpha}(\vec{q},t)+i\mathbf{q}^{\alpha}\mathbf{J}^{\alpha}(\vec{q})\mathbf{S}^{-1}(\vec{q},0)\mathbf{S}(\vec{q},t)+\mathbf{J}^{\alpha}(\vec{q})\int_0^t dt'\sum_{\alpha'}\mathbf{m}^{\alpha\alpha'}(\vec{q},t-t')\mathbf{S}^{\alpha'}(\vec{q},t')=0. \tag{1b}$$

with initial conditions

$$\mathbf{S}(\vec{q},0)\equiv\mathbf{S}(\vec{q}), \tag{2}$$

$$\dot{\mathbf{S}}(\vec{q},0)\equiv 0\equiv\mathbf{S}^{\alpha}(\vec{q},0), \tag{3}$$

$$\dot{\mathbf{S}}^{\alpha}(\vec{q},0)\equiv -i\mathbf{J}^{\alpha}(\vec{q})\mathbf{q}^{\alpha}, \tag{4}$$

$$(\mathbf{q}^{\alpha})_{lm,l'm'}=q_l^{\alpha}(\vec{q})\,\delta_{ll'}\delta_{mm'}, \tag{5}$$

$$q_l^{\alpha}(\vec{q}):=\begin{cases} q, & \alpha=T\ \ \forall\ \ l,\\ \sqrt{l(l+1)}, & \alpha=R\ \ \forall\ \ \vec{q}, \end{cases} \tag{6}$$

$$(\mathbf{J}^{\alpha}(\vec{q}))_{lm,l'm'}\equiv J^{\alpha\alpha'}_{lm,l'm'}(\vec{q})=\frac{k_BT}{I^{\alpha}}\delta_{\alpha\alpha'}\delta_{ll'}\delta_{mm'}, \tag{7}$$

and the density–current-density correlator:

$$S^{\alpha}_{lm,l'm'}(\vec{q},t)=\frac{1}{N}\langle j^{\alpha *}_{lm}(\vec{q},t)\,\delta\rho_{l'm'}(\vec{q},0)\rangle. \tag{8}$$

Here, $\mathbf{S}(\vec{q})$ and $\mathbf{J}^{\alpha\alpha'}(\vec{q})$ denote, respectively, the static density and current density correlation matrix and

$$I^{\alpha}=\begin{cases} M, & \alpha=T,\\ I, & \alpha=R. \end{cases} \tag{9}$$

This set of equations is still exact, but needs an expression for the memory kernels $m^{\alpha\alpha'}_{lm,l'm'}(\vec{q},t)$. This is where approximations come in. Their nature depends strongly on the physical situation: for example, $\mathbf{m}^{\alpha\alpha'}$ for a supercooled liquid will be quite different from that for a liquid at higher temperatures. We also note that instead of choosing the scalar current densities one could also use each Cartesian component $j^{\alpha i}_{lm}$, $i=x,y,z$, as a slow variable. This was done recently for $\alpha=T$ but not for $\alpha=R$ in order to discuss the role of transverse currents on light scattering spectra [68]. The resulting equations again are exact but involve memory kernels $m^{\alpha i,\alpha' i}_{lm,l'm'}(\vec{q},t)$.

B. Linearized equations of motion

Since the memory kernels will not be independent functions of the tensorial density correlations $\mathbf{S}(\vec{q},t)$, the third term in Eq. (1b) is a kind of *nonlinearity*. Within MCT $\mathbf{m}^{\alpha\alpha'}(\vec{q},t)$ is approximated by superpositions of products $\mathbf{S}(\vec{q}_1,t)\mathbf{S}(\vec{q}_2,t)$ with $\vec{q}=\vec{q}_1+\vec{q}_2$, which makes obvious the nonlinear character of the equations of motion. It is this nonlinearity that leads to a slowing down of the structural relaxation by decreasing the temperature or increasing the density of a liquid. This behavior takes place on the liquid side as a two-step relaxation process characterized by two diverging time scales $t_{\sigma}\sim|T-T_c|^{-1/2a}$ and $\tau\sim(T-T_c)^{-\gamma}$ where a and γ are positive and T_c is the ideal glass transition temperature. The time scale for t_{σ} and τ is determined by a microscope scale t_0. t_0 depends on inertia and damping effects

where the latter are due to the regular part of $\mathbf{m}^{\alpha\alpha'}(\vec{q},t)$, accounting for the fast motions. Because our main interest is the microscopic dynamics, we can get an estimate of the microscopic time scale by neglecting the memory term including its regular part. This results in a set of linear equations from which one immediately obtains for the normalized correlator $\mathbf{\Phi}(\vec{q},t)=\mathbf{S}^{-1/2}(\vec{q})\mathbf{S}(\vec{q},t)\mathbf{S}^{-1/2}(\vec{q})$

$$\ddot{\mathbf{\Phi}}(\vec{q},t)+\mathbf{\Omega}^2(\vec{q})\mathbf{\Phi}(\vec{q},t)=0, \tag{10}$$

with initial conditions

$$\mathbf{\Phi}(\vec{q},0)=\mathbf{1}, \quad \dot{\mathbf{\Phi}}(\vec{q},0)=\mathbf{0} \tag{11}$$

and the Hermitian frequency matrix squared

$$\mathbf{\Omega}^2(\vec{q})=\mathbf{S}^{-1/2}(\vec{q})\sum_{\alpha}(\mathbf{q}^{\alpha})^2\mathbf{J}^{\alpha}\mathbf{S}^{-1/2}(\vec{q}) \tag{12}$$

or with Eqs. (5), (6), and (9)

$$(\mathbf{\Omega}^2(\vec{q}))_{lm\cdot l'm'}=\sum_{l''m''}(\mathbf{S}^{-1/2}(\vec{q}))_{lm,l''m''}\left[\frac{k_BT}{M}q^2+\frac{k_BT}{I}l''\times(l''+1)\right](\mathbf{S}^{-1/2}(\vec{q}))_{l''m'',l'm'}. \tag{13}$$

Here, some comments are in order. First, the static correlators $S_{lm,l'm'}(\vec{q})$ and therefore $\Omega_{lm,l'm'}(\vec{q})$ are not diagonal in l and l' in general. Accordingly, translational and rotational modes generally are coupled to each other for given $\vec{q}$. Second, this coupling vanishes in the limit $q\to 0$, because the static correlators $S_{lm,l'm'}(\vec{q})$ and therefore $\Omega_{lm,l'm'}(\vec{q})$ [cf. Eq. (13)] become diagonal and independent of each other for an isotropic liquid:

$$\Omega_{lm,l'm'}(\vec{q})\to\omega_l(q)\delta_{ll'}\delta_{mm'} \tag{14}$$

with

$$\omega_0(q)=\sqrt{\frac{k_BT}{MS_0}}q, \tag{15a}$$

$$\omega_l(q)=\sqrt{\frac{k_BT}{IS_l}}\sqrt{l(l+1)}, \quad l>0, \tag{15b}$$

the translational and rotational frequencies for $q\to 0$ and $S_l\equiv S_{l0,l0}(\vec{q}=0)$. $\omega_0(q)$ describes the well known *acoustic* isothermal sound wave dispersion and $\omega_l(q)$ the *optic* rotational frequencies for $l>0$.

Third, the limit $q\to 0$ was already discussed for a molecular liquid using a *site-site* description [69]. These authors also set the corresponding memory matrix to zero, which, by the way, is completely equivalent to a short time expansion of the equation of motion in leading order. But there the coupling between the partial dynamical structure factors does not vanish for $q\to 0$. In this respect the choice of a molecular representation that takes care of the isotropy of the microscopic Hamiltonian is the most natural one, at least for $q\to 0$ and $t\to 0$.

So far we have considered the *liquid* phase only. The idealized version of MCT, which neglects so-called hopping processes, is a theory developed on the liquid side of the glass transition, because it uses as an input static correlators in equilibrium. It may also be used below, but close to the transition point where the singular behavior still dominates. Whether MCT is even capable of describing dynamical features far below the glass transition point is unclear. Nevertheless, we will also apply MCT for parameters deeper in the *glass* phase. An ideal glass is a nonergodic phase with nonergodicity parameters (not normalized)

$$F_{lm,l'm'}(\vec{q})=\lim_{t\to\infty}S_{lm,l'm'}(\vec{q},t) \tag{16}$$

that are nonzero. One can easily prove that Eqs. (1b) then imply that

$$C^{\alpha\alpha'}_{lm,l'm'}(\vec{q})=\lim_{t\to\infty}m^{\alpha\alpha'}_{lm,l'm'}(\vec{q},t) \tag{17}$$

are nonzero too, and that

$$\sum_{\alpha,\alpha'}\mathbf{q}^{\alpha}\{[\mathbf{C}^{\beta\beta'}(\vec{q})]^{-1}\}^{\alpha\alpha'}\mathbf{q}^{\alpha'}=[\mathbf{S}(\vec{q})-\mathbf{F}(\vec{q})]\mathbf{F}^{-1}(\vec{q})\mathbf{S}(\vec{q}). \tag{18}$$

Therefore, we introduce $\hat{\mathbf{S}}(\vec{q},t)$ and $\hat{\mathbf{m}}^{\alpha\alpha'}(\vec{q},t)$ such that

$$\mathbf{S}(\vec{q},t)=\mathbf{F}(\vec{q})+\hat{\mathbf{S}}(\vec{q},t), \tag{19}$$

$$\mathbf{m}^{\alpha\alpha'}(\vec{q},t)=\mathbf{C}^{\alpha\alpha'}(\vec{q})+\hat{\mathbf{m}}^{\alpha\alpha'}(\vec{q},t), \tag{20}$$

in analogy with the approach in [57]. Substitution of Eq. (19) and Eq. (20) into Eq. (1) yields

$$\ddot{\hat{\mathbf{S}}}(\vec{q},t)+i\sum_{\alpha}\mathbf{q}^{\alpha}\mathbf{S}^{\alpha}(\vec{q},t)=0, \tag{21a}$$

$$\dot{\mathbf{S}}^{\alpha}(\vec{q},t)+i\mathbf{q}^{\alpha}\mathbf{J}^{\alpha}(\vec{q})\mathbf{S}^{-1}(\vec{q})\hat{\mathbf{S}}(\vec{q},t)+\mathbf{J}^{\alpha}(\vec{q})\int_0^t dt'\sum_{\alpha'}\hat{\mathbf{m}}^{\alpha\alpha'}(\vec{q},t-t')\mathbf{S}^{\alpha'}(\vec{q},t')+i\mathbf{q}^{\alpha}\mathbf{J}^{\alpha}(\vec{q})\mathbf{S}^{-1}(\vec{q})\mathbf{F}(\vec{q})+\mathbf{J}^{\alpha}(\vec{q})\sum_{\alpha'}\mathbf{C}^{\alpha\alpha'}(\vec{q})\int_0^t dt'\mathbf{S}^{\alpha'}(\vec{q},t')=0 \tag{21b}$$

with initial conditions

$$\hat{\mathbf{S}}(\vec{q},0)=\mathbf{S}(\vec{q})-\mathbf{F}(\vec{q}) \tag{22}$$

and

$$\lim_{t\to\infty}\hat{\mathbf{S}}(\vec{q},t)=0, \quad \lim_{t\to\infty}\hat{\mathbf{m}}^{\alpha\alpha'}(\vec{q},t)=0. \tag{23}$$

With the same argumentation as above we linearize Eqs. (21b) by taking $\hat{\mathbf{m}}^{\alpha\alpha'}(\vec{q},t)$ to be zero. Then, taking the time derivative of Eq. (21b) and using Eq. (21a) we get for $\hat{\mathbf{S}}^{\alpha}(\vec{q},t) \equiv (\mathbf{J}^{\alpha}(\vec{q}))^{-1/2}\mathbf{S}^{\alpha}(\vec{q},t)$

$$\ddot{\hat{\mathbf{S}}}^{\alpha}(\vec{q},t) + \sum_{\alpha'} (\hat{\mathbf{\Omega}}^2(\vec{q}))^{\alpha\alpha'}\hat{\mathbf{S}}^{\alpha'}(\vec{q},t) = 0 \tag{24}$$

with the frequency matrix squared

$$\hat{\mathbf{\Omega}}^2(\vec{q})^{\alpha\alpha'} = (\mathbf{J}^{\alpha}(\vec{q}))^{1/2}[\mathbf{q}^{\alpha}\mathbf{S}^{-1}(\vec{q})\mathbf{q}^{\alpha'} - \mathbf{C}^{\alpha\alpha'}(\vec{q})](\mathbf{J}^{\alpha'}(\vec{q}))^{1/2}. \tag{25}$$

Integration of Eq. (21a) from 0 to t and substituting $\int_0^t dt' \mathbf{S}^{\alpha'}(\vec{q},t')$ from Eqs. (21b) with $\hat{\mathbf{m}}^{\alpha\alpha'} \equiv 0$ allows one to express $\hat{\mathbf{S}}(\vec{q},t)$ by $\hat{\mathbf{S}}^{\alpha}(\vec{q},t)$:

$$\hat{\mathbf{S}}(\vec{q},t) = i\mathbf{F}(\vec{q})\mathbf{S}^{-1}(\vec{q}) \sum_{\alpha,\alpha'} \mathbf{q}^{\alpha}[(\mathbf{C}^{\beta\beta'}(\vec{q}))^{-1}]^{\alpha\alpha'} \times (\mathbf{J}^{\alpha'}(\vec{q}))^{1/2}\hat{\mathbf{S}}^{\alpha'}(\vec{q},t) \tag{26}$$

Like $\mathbf{\Omega}$, the matrix $(\hat{\mathbf{\Omega}}^{\alpha\alpha'})$ is nondiagonal in l,l' and in α, α'. This again leads to a coupling between the translational and orientational modes, which are the eigenmodes of $(\hat{\mathbf{\Omega}}^{\alpha\alpha'})$. Now it is (see [6])

$$\mathbf{C}^{\alpha\alpha'}(\vec{q}) = \tilde{\mathbf{q}}^{\alpha}\tilde{\mathbf{C}}^{\alpha\alpha'}(\vec{q})\tilde{\mathbf{q}}^{\alpha'} \tag{27}$$

with

$$\lim_{\vec{q}\to 0} \tilde{C}^{\alpha\alpha'}_{lm,l'm'}(\vec{q}) \neq 0 \tag{28}$$

and

$$(\tilde{\mathbf{q}}^{\alpha})_{lm,l'm'} = \tilde{q}^{\alpha}_{lml'm'} = \tilde{q}^{\alpha}_{l}\delta_{ll'}\delta_{mm'}, \tag{29}$$

$$\tilde{q}^{\alpha}_{l} = \begin{cases} q, & (\alpha,l) = (T,0), \\ 1, & (\alpha,l) \neq (T,0), \end{cases} \tag{30}$$

not to be confused with $\mathbf{q}^{\alpha}$. Therefore, we get from Eq. (25) with Eqs. (5), (6), (27), and (29),

$$(\hat{\mathbf{\Omega}}^{\,2}(\vec{q}))^{TT}_{00,00} = \frac{k_B T}{M} q^2 (\mathbf{S}^{-1}(\vec{q}))_{00,00}[1 + (\mathbf{S}(\vec{q})\tilde{\mathbf{C}}^{TT}(\vec{q}))_{00,00}] \tag{31}$$

for the acoustic part of $((\hat{\Omega}^2)^{\alpha\alpha'})$. Taking into account that we have not normalized $\mathbf{C}^{\alpha\alpha'}$ and $\tilde{\mathbf{C}}^{\alpha\alpha'}$, the result Eq. (31) is completely analogous to the result derived in [57] for $(\hat{\mathbf{\Omega}}(\vec{q}))^2$ for simple one-component liquids. However, we note that in contrast to [57] the equations of motion for the rescaled correlators $\hat{\mathbf{S}}(\vec{q},t)$ and $\hat{\mathbf{m}}^{\alpha\alpha'}(\vec{q},t)$ are not covariant, due to the splitting of the current density into a translational and a rotational part. Therefore $(\hat{\mathbf{\Omega}}^2(\vec{q}))^{\alpha\alpha'}$ is not a straightforward generalization of $\hat{\mathbf{\Omega}}^2(\vec{q})$ for simple liquids to molecular liquids.

The coupling between translational and orientational modes in the liquid and in the glass already on the linear level of the equations of motion is not surprising due to the interaction between translational and orientational degrees of freedom. But it is also obvious that memory effects will lead to additional couplings, and it is this point, that we will investigate in Sec. III.

C. Mode-coupling theory

In the preceding subsection we have neglected the memory kernels. Approaching the glass transition significant memory effects occur. Therefore $\mathbf{m}^{\alpha\alpha'}$ must be taken into account. Using mode-coupling theory an approximate expression for the slow part $\mathbf{m}^{\alpha\alpha'}(\vec{q},t)$ has been derived which leads to a closed set of equations for $\mathbf{S}(\vec{q},t)$. This has been done for molecular systems using the molecular representation [5–7] and a site-site description [67]. For a liquid of linear molecules we will use

$$m^{\alpha\alpha'}_{lm,l'm'}(\vec{q},t) \approx \frac{\sqrt{I_{\alpha}I_{\alpha'}}}{k_B T}\Gamma^{\alpha\alpha'}_{lm,l'm'}(\vec{q})\,\delta(t) + (m^{\alpha\alpha'}_{lm,l'm'}(\vec{q},t))_{\text{slow}} \tag{32}$$

where the first and second terms on the right-hand side of Eq. (32) accounts for the fast and the slow contributions, respectively. MCT yields [6]

$$(m^{\alpha\alpha'}_{lm,l'm'}(\vec{q},t))_{\text{slow}} = \frac{1}{2N} \sum_{\substack{\vec{q}_1\vec{q}_2 \\ \vec{q}_1+\vec{q}_2=\vec{q}}} \sum_{\substack{l_1m_1 \\ l_2m_2}} \sum_{\substack{l_1'm_1' \\ l_2'm_2'}} V^{\alpha\alpha'}_{lm,l'm'}(\vec{q}|\vec{q}_1 l_1 m_1, l_1' m_1'; \vec{q}_2 l_2 m_2, l_2' m_2') S_{l_1m_1,l_1'm_1'}(\vec{q}_1,t) S_{l_2m_2,l_2'm_2'}(\vec{q}_2,t). \tag{33}$$

The explicit expressions for the vertices $\mathbf{V}$ are given in Ref. [6]. Equations (1) together with Eqs. (32) and (33) are a closed set of equations for $S_{lm,l'm'}(\vec{q},t)$ which need the damping coefficients $\Gamma^{\alpha\alpha'}_{lm,l'm'}(\vec{q})$ and the static correlators $S_{lm,l'm'}(\vec{q})$ as a input. The latter uniquely determine the vertices.

It is obvious that the MCT polynomial $(m^{\alpha\alpha'}_{lm,l'm'})_{\text{slow}}$ leads to additional coupling between the correlators $S_{lm,l'm'}(\vec{q},t)$.

Due to this nonlinearity the MCT equations (1), (32), and (33) can only be solved numerically. We have performed such a numerical solution for dipolar hard spheres, one of the simplest systems involving translational and rotational motion.

D. Dipolar hard sphere liquid

The investigation of dipolar hard spheres has the advantage that approximate analytical expressions [70] for the static correlators are known.

We consider a system of N hard spheres with homogeneous number density ρ, diameter d, mass M, moment of inertia $I=\frac{1}{10}Md^2$, and dipolar moment μ. The origin of the body-fixed frame is chosen to coincide with the center of mass of each sphere, which is the natural choice. Since the density of the particles is homogeneous, the center of mass is equal to the center of the spheres. The reader should note that the MCT equations (1), (32), and (33) and even the original exact equations of motion Eqs. (1) are not covariant (i.e., invariant in their form) under a shift of the reference point for the body-fixed frame. In order to get covariant equations one has to project on the individual Cartesian components of $\vec{j}^{T}_{lm}(\vec{q})$ and $\vec{j}^{R}_{lm}(\vec{q})$. Nevertheless, we think that the present equations are a reasonably good approach to the dynamics of molecular liquids, because of the natural choice of the reference frame. Of course, this point needs additional investigation. The advantage of MCT in site-site representation [67] is that this problem does not occur, because no reference point must be chosen.

The physical control parameters are the packing fraction $\phi=(\pi/6)\rho d^3$ and the temperature T. In the following the length unit is chosen such that $d=1$. In addition we choose $M=1$ and $\mu=1$. This choice means that time t and temperature T are measured in units of $M^{1/2}d^{5/2}/\mu$ and $k_B^{-1}\mu^2/d^3$, respectively. In the following we will use $T^*=T/(\mu^2/k_Bd^3)$ as dimensionless temperature.

As already stated, the MCT equations (1), (32), and (33) require $\Gamma^{\alpha\alpha'}_{lm,l'm'}(\vec{q})$ and $S_{lm,l'm'}(\vec{q})$ as input. Throughout this paper we will put all damping coefficients $\Gamma^{\alpha\alpha'}_{lm,l'm'}$ to zero. The static correlators $S_{lm,l'm'}(\vec{q})$ are obtained from Wertheim's solution, who used the Percus-Yevick and mean spherical approximations [70] This leads to

$$S_{lm,l'm'}(\vec{q})\approx\begin{cases} S_{lm}(q)\,\delta_{ll'}\delta_{mm'}, & l=0,1,\quad l'=0,1,\\ \delta_{ll'}\delta_{mm'} & \text{otherwise.}\end{cases} \tag{34}$$

The vertices of the memory kernels are bilinear in the direct correlation functions:

$$c_{lm}(q)=\frac{4\pi}{\rho}\left[1-\frac{1}{S_{lm}(q)}\right]. \tag{35}$$

Since we have chosen the so-called q frame [71] [for which $\vec{q}=\vec{q}_0\equiv(0,0,q)$] the correlators and the kernels become diagonal in m and m' [6]. The fact that the static correlators are diagonal in l and l' and are structureless for $l,\quad l'\geqslant 2$ is an artifact of both approximations. Additional shortcomings are (i) the independence of the center of mass correlator $S_{00}(q)$ of temperature and (ii) the smooth behavior of $S_{lm}(q)$ at $\phi_{\rm rcp}\simeq 0.64$, the value for random close packing. The static correlators from Wertheim's approach exhibit a divergency at $\phi=\phi_{\max}=1$, only. We will come back to these points below.

Due to Eqs. (34) and (35) mode coupling occurs only between the time-dependent correlators with l_1,l_1',l_2,l_2' smaller than or equal to 1. In order to simplify the MCT equations as much as possible we use the additional approximations (in the q frame)

$$S_{lm,l'm'}(\vec{q},t)\approx\begin{cases} S_{lm}(q,t)\,\delta_{ll'}\delta_{mm'}, & l=0,1,l'=0,1,\\ 0 \quad \text{otherwise,}\end{cases} \tag{36}$$

$$m^{\alpha\alpha'}_{lm,l'm'}(\vec{q},t)\approx\begin{cases} m^{\alpha\alpha'}_{lm}(q,t)\,\delta_{ll'}\delta_{mm'}, & l=0,1,l'=0,1,\\ 0 \quad \text{otherwise.}\end{cases} \tag{37}$$

In Sec. II B we showed that the translational and orientational dynamics is already coupled on the linear level due to nondiagonality in l and l'. Above we have chosen all correlators to be diagonal in l and l'. Thus a coupling between $S_{00}(q,t)$ and $S_{lm}(q,t)$ with $l>0$ can originate only from mode-coupling effects. Thus, our diagonalization approximation (which is even exact in our case due to the restriction of l and l' to 0 and 1) allows us to study the influence of the mode-coupling terms on the microscopic dynamics without interfering with the direct coupling mechanism between the correlators $S_{lm}(q,t)$ discussed in Sec. II B.

The memory kernels [cf. Eq. (33)] in the q frame $m^{\alpha\alpha'}_{lm,l'm'}(\vec{q},t)=m^{\alpha\alpha'}_{lm}(q,t)\,\delta_{ll'}\delta_{mm'}$ contain the following couplings [6]:

$$m^{\alpha\alpha'}_{00}(q,t)\leftrightarrow S_{00}(q_1,t)S_{00}(q_2,t)\quad\text{and}$$
$$S_{1m_1}(q_1,t)S_{1m_2}(q_2,t), \tag{38}$$

$$m^{\alpha\alpha'}_{1m}(q,t)\leftrightarrow S_{00}(q_1,t)S_{1m_2}(q_2,t)\quad\text{and}$$
$$S_{1m_1}(q_1,t)S_{00}(q_2,t). \tag{39}$$

Equation (38) shows that the center of mass correlator $S_{00}(q,t)$ may undergo a glass transition independently from the dipoles whereas Eq. (39) demonstrates that the dipoles are ''slaved'' by the center of mass dynamics and can freeze only if $S_{00}(q,t)$ has become nonergodic. In order that $S_{00}(q,t)$ and $S_{1m}(q,t)$ freeze simultaneously the vertices of the bilinear terms in Eq. (39) must be large enough. This happens at low enough temperatures. Since $S_{l,-m}(q,t)\equiv S_{l,m}(q,t)$ [6], there are three independent correlators, the center of mass correlation function $S_{00}(q,t)$ and two dipolar ones $S_{1m}(q,t),\quad m=0,1$. In the following we consider the normalized correlators $\phi_{lm}(q,t)=S_{lm}(q,t)/S_{lm}(q)$.

The three static correlators are shown in Fig. 1 for two different pairs of (ϕ,T^*). Three main features can be seen.

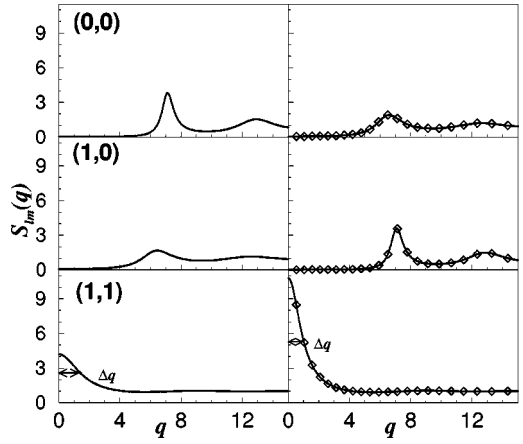

FIG. 1. The q dependence of the static structure factors $S_{lm}(q)$ for $(lm)=(0,0),(1,0),(1,1)$ and two different pairs of (ϕ,T^*) indicated by the full circles in Fig. 2 below: (0.53,0.3) (left), (0.381,0.04) (right). Δq is the peak width of $S_{11}(q)$ at half maximum. The symbols indicate the discretized q values (see text).

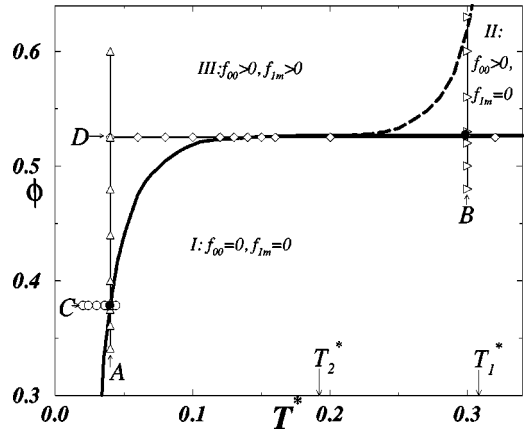

FIG. 2. Glass transition phase diagram for dipolar hard spheres: The solid and the dashed line are critical lines at which a discontinuous (type B) and a continuous (type A) glass transition takes place between the phases I, II, and III. A, B, C, and D denote the various paths on which we have investigated the control parameter dependence of the dynamics. The full circles indicate the two points at which the static correlators in Fig. 1 and the microscopic frequencies in Fig. 3 below were calculated. For T_1^* and T_2^*, see text.

First, the q variations of S_{00} of the ''longitudinal'' dipolar correlator and of S_{10} are rather similar to each other and resemble that of a simple liquid with a well pronounced main peak at $q_{\max}\approx 2\pi/\bar{a}$, where $\bar{a}\approx d=1$, the mean distance between nearest neighbors. The ''transverse'' dipolar correlator $S_{11}(q)$ behaves quite differently. It exhibits only one peak, at $q=0$, and it becomes almost structureless for $q>\triangle q$, the peak width at half maximum. Second, $S_{11}(q=0)$ increases with decreasing temperature, whereas $\triangle q$ decreases. This behavior signals medium range orientational order due to a precursor of ferrofluid order. This order is induced by enhancement of the dipolar interactions at lower temperatures with respect to the hard core repulsion. Third, $S_{1m}(q=0)$ depends on m, because of the long range nature of the dipolar interactions.

In addition to the truncation at $l=1$ we must also truncate and discretize the q variable. Since the reduction (for $N\rightarrow\infty$) to a single integral of the sum over $\vec{q}_1$ and $\vec{q}_2$ in Eq. (33) for simple liquids [72] cannot easily be used for molecular liquids the number of steps to calculate this sum increases quadratically with the number of q values, instead of the linear increase for simple liquids. This fact makes the numerical solution of the molecular MCT equations rather CPU time consuming. Therefore we decided to choose a nonequidistant distribution of 30 q values between $q_{low}\simeq 0.51$ and $q_{up}\simeq 40$. These values were generated by the nonlinear relation

$$q_\nu=\frac{1}{\alpha}\operatorname{arctanh}(\nu\Delta_x),\qquad \nu=1,2,\ldots,30, \tag{40}$$

with $\Delta_x=\tanh(\alpha q_{co})/31$ and $q_{co}=50$. The parameter α has been chosen such that the main peak of, e.g., $S_{00}(q)$, is still in the linear regime of arctanh. The right of Fig. 1 demonstrates this for $\alpha=0.065$. It is obvious from Eq. (40) that for $q<\alpha^{-1}$ the q_ν are almost equidistant and for $q>\alpha^{-1}$ they become more and more diluted. Since the large q regime is not as important as the range around the main peak in $S_{00}(q)$ or that at $q=0$ in $S_{11}(q)$ (which drive the glass transition) our choice for q_ν should not influence our results, at least qualitatively. We have solved the molecular MCT equations (1), (32), and (33) in time space using an algorithm already developed to solve the MCT equations for simple liquids [73]. However, our numerical procedure differs from that of Götze *et al.* [74] for the single dumbbell in an isotropic liquid. These authors introduced an effective memory kernel (independent of α and α') and an effective microscopic frequency.

Before we come to the dynamics let us briefly discuss the phase diagram for a glass transition that has already been calculated [6,75]. Throughout the rest of this paper all the results are given in the q frame. The modification with respect to Refs. [6,75] of the q discretization leads to a small quantitative change of the glass transition lines, but without changing the topology. Therefore we have again calculated the nonergodicity parameters

$$f_{lm}(q)=\lim_{t\rightarrow\infty}\phi_{lm}(q,t) \tag{41}$$

as a function of ϕ and T^*, from which the phase diagram is obtained (Fig. 2). Since ϕ cannot exceed $\phi_{rcp}\simeq 0.64$, the value for random close packing of hard spheres, we have plotted only $\phi\leqslant\phi_{rcp}$. There are two significant temperatures T_1^* and T_2^*. At T_1^* the critical line $\phi^c_{\text{type }A}(T^*)$ (dashed line in Fig. 2) reaches $\phi=\phi_{rcp}$ and at T_2^* it merges into the critical line $\phi^c_{\text{type }B}(T^*)$ (solid line in Fig. 2). These two temperatures have the following meaning. For $T^*>T_1^*$ an increase of ϕ leads at $\phi^c_{\text{type }B}(T^*)$ to a glass transition for the center of mass motion, but not for the dipoles. Choosing T^* between T_1^* and T_2^*, again a glass transition of the center of mass motion occurs at $\phi^c_{\text{type }B}(T^*)$. But on increasing ϕ beyond $\phi^c_{\text{type }B}(T^*)$ a spin-glass-like transition for the dipoles

occurs at $\phi^c_{\text{type }A}(T^*)$. Below T_2^*, center of mass and dipolar dynamics freeze simultaneously at $\phi^c_{\text{type }B}(T^*)$. For $T^* > T_2^*$ the critical value $\phi^c_{\text{type B}}(T^*)$ is identical to that for hard spheres ϕ^c_{HS}. For the present choice of q discretization we find $\phi^c_{HS} \simeq 0.5265$, which does not differ much from the more precise value $\phi^c_{HS} \simeq 0.516$ obtained with 100 equidistant q values [76].

The glass transition at high and low temperatures is driven by different physical mechanisms. At high temperatures it is the so-called cage effect, which leads to the freezing of the liquid into a nonergodic phase, due to an increase with increasing density of the main peak of the center of mass correlator $S_{00}(q)$. Lowering the temperature enhances the role of the dipolar interactions, which leads to a strong increase of the peak at $q=0$ of the ''transverse'' dipolar correlator $S_{11}(q)$. The increase of the dipolar correlations is accompanied by a decrease of the center of mass correlations (cf. Fig. 1), and they take over the role of the cage effect. This behavior is reflected in the nonergodicity parameters. $f_{11}(q=0)$ increases with decreasing temperature much more strongly than $f_{00}(q_{\max})$. For details the reader is referred to [6].

The properties of the phase diagram require some more comments. (i) the T^* independence of $\phi^c_{\text{type }B}(T^*)$ for $T^* > T_1^*$ originates from the T^* independence of $S_{00}(q)$, which is an artifact of Wertheim's solution. Removing this artifact will result in a T^* dependence of $\phi^c_{\text{type }B}(T)$ for *all* T^* with $\lim_{T^*\to\infty} \phi^c_{\text{type }B}(T^*) = \phi^c_{HS}$, since dipolar interactions will be irrelevant at infinite temperature. (ii) The existence of T_1^* relies on the fact that $\phi^c_{\text{type }A}(T^*)$ approaches the value ϕ_{rcp} at a finite temperature. This is true when the static correlators within the Percus-Yevick approximation are used. Whether or not an improved theory reproducing the singular behavior at ϕ_{rcp} would lead to the same conclusion is not obvious. Since such a theory does not exist, we cannot exclude the possibilities that $\phi^c_{\text{type }A}(T^*)$ approaches ϕ_{rcp} only at $T^* = \infty$.

Now we turn to the time- or frequency-dependent features of dipolar hard spheres. We have studied the control parameter dependence of the dynamics along the paths *A*, *B*, *C*, and *D*, indicated in Fig. 2. In contrast to the determination of the long time behavior, inertia effects will play an important role in the microscopic time or frequency regime. In the liquid, these inertia effects enter through the microscopic frequency matrix $\Omega(\vec{q})$. Due to the diagonality of $\mathbf{S}(\vec{q})$ the matrix $\mathbf{\Omega}(\vec{q})$ becomes diagonal with diagonal elements (in the q frame) that follow from Eq. (13):

$$\Omega_{lm}(q) = \sqrt{\left[\frac{k_B T}{M} q^2 + \frac{k_B T}{I} l(l+1)\right] \Big/ S_{lm}(q)}, \quad (42)$$

restricted to $l=0,1$. Figure 3 depicts $\Omega_{lm}(q)$ for two different pairs (ϕ, T^*) in the vicinity of the critical line $\phi^c_{\text{type }B}(T^*)$. This figure reveals two features which stem from the properties of $S_{lm}(q)$ discussed above. First, $\Omega_{1m}(q=0)$ depends on m. Second, and most important, a ''softening'' of the ''optic'' frequency $\Omega_{11}(q)$ with $q\to 0$ is

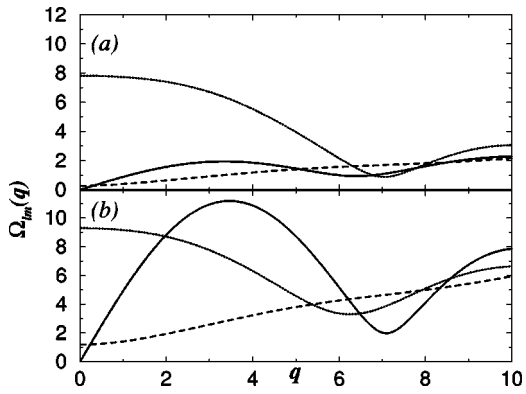

FIG. 3. q dependence of the microscopic frequencies $\Omega_{lm}(q)$ for $(l,m)=(0,0)$ (solid), (1,0) (dotted), and (1,1) (dashed). (a) $\phi = 0.381$, $T^*=0.04$ and (b) $\phi=0.53$, $T^*=0.3$, indicated in Fig. 2 by the full circles.

observed for decreasing temperature T^*, for which the role of dipolar interactions (compared to the hard core repulsion) becomes more and more enhanced. This ''softening'' comes from the strong increase of $S_{11}(q)$ for $q\to 0$ (see Fig. 1) and has its physical origin in the occurrence of a medium range orientational order of the dipoles. The inverse width $(\Delta q)^{-1}$ of the peak in $S_{11}(q)$ at $q=0$ is a measure of the length scale of this orientational order. $(\Delta q)^{-1}$ increases with decreasing temperature (see Fig. 1). We will come back to this point in the final section.

The microscopic frequencies in the glass phase are given by the ''renormalized'' frequency matrix $[(\hat{\Omega}^2(\vec{q}))^{\alpha\alpha'}]$. Taking again into account the diagonalization with respect to l and l' we obtain from Eq. (25) with Eqs. (5) and (27)

$$(\hat{\mathbf{\Omega}}^2_{lm}(q))^{\alpha\alpha'} = \frac{k_B T}{(I_\alpha I'_\alpha)^{1/2}} \frac{1}{S_{lm}(q)} \times [q_l^\alpha q_l^{\alpha'} + \tilde{q}_l^\alpha \tilde{q}_l^{\alpha'} \tilde{C}^{\alpha\alpha'}_{lm}(q) S_{lm}(q)]. \quad (43)$$

Since $\tilde{C}^{\alpha\alpha'}_{00}(q)$ is different from zero for $\alpha=\alpha'=T$ only, we get with Eqs. (6), (18), (27), and (29):

$$\hat{\mathbf{\Omega}}_{00}(q) = \Omega_{00}(q)/[1-f_{00}(q)]^{1/2}. \quad (44)$$

$\tilde{C}^{\alpha\alpha'}_{1m}(q)$ is nonzero for all (α, α'). Therefore two eigenfrequencies $\hat{\Omega}^{\pm}_{1m}(q)$ exist for each m. $\hat{\mathbf{\Omega}}_{00}(q)$ and $\hat{\Omega}^{\pm}_{1m}(q)$ are shown in Fig. 4. The ''renormalized'' frequencies require the nonergodicity parameters as input. The latter become less accurate for small q, because the discretization of the q values influences the results much more strongly for decreasing q. Therefore we do not present data below $q=1$. Of course, $\hat{\Omega}_{00}(q) \to \hat{c}q$ and $\hat{\Omega}^{\pm}_{1m}(q) \to \hat{\Omega}^{\pm}_{1m}(0) > 0$ for $q\to 0$. Note that (i) $\hat{\Omega}^{\pm}_{11}(q)$ does not vary much with q and (ii) $\hat{\Omega}^{-}_{11}(q) \ll \hat{\Omega}_{00}(q_{max} \simeq 7)$.

Now let us turn to Eq. (1) including the time-dependent memory kernels given by Eqs. (32) and (33). From the solutions of these MCT equations we get the normalized correla-

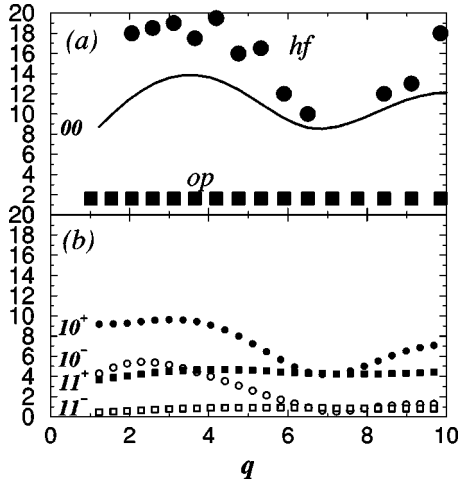

FIG. 4. q dependence of the renormalized microscopic frequencies for $\phi=0.53$, $T^*=0.04$. (a) $\hat{\Omega}_{00}(q)$ is shown as solid line; the positions $\hat{\omega}_{hf}$ and $\hat{\omega}_{op}$ obtained from $\phi''_{00}(q,\omega)$ are presented by the full circles and squares, respectively. (b) $\hat{\Omega}^{\pm}_{10}(q)$ and $\hat{\Omega}^{\pm}_{11}(q)$ are shown as circles and squares, respectively.

tors $\phi_{lm}(q,t)$ or equivalently the corresponding susceptibility spectra $\chi''_{lm}(q,\omega)$ related to the correlation spectra $\phi''_{lm}(q,\omega)$ by $\chi''_{lm}(q,\omega)=\omega\phi''_{lm}(q,\omega)$. Figures 5 and 6 show $\phi_{lm}(q,t)$ and $\chi''_{lm}(q,\omega)$ for $q\simeq 4.7$ along path A in Fig. 2. Figure 5 clearly demonstrates for all correlators the formation of a plateau and the tremendous slowing down of the relaxation with increasing ϕ, which stops at $\phi_c(T^*)\simeq 0.3782$.

The dynamical features are better recognized in ω space. Before we discuss these results, let us comment on the quality of our ω-dependent data. Because glassy dynamics involves many decades in time one has to use a special algorithm, which decimates the time step with increasing time, i.e., one chooses an initial time increment h to discretize the

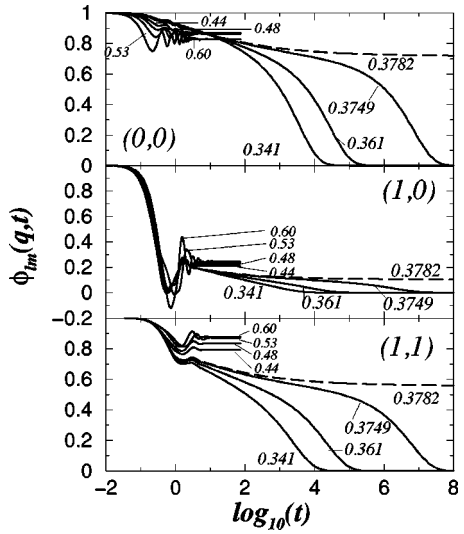

FIG. 5. Linear-logarithmic plot of $\phi_{lm}(q,t)$ at $q\simeq 4.7$, $T^*_A=0.04$, and ϕ along path A in Fig. 2. The dashed line corresponds to the results at $\phi\simeq\phi_c\simeq 0.3782$.

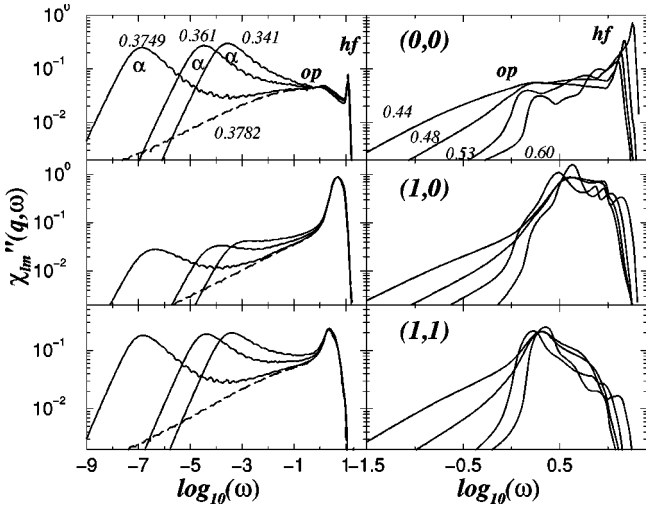

FIG. 6. Log-log plot of $\chi''_{lm}(q,\omega)$ at $q\simeq 4.7$, $T^*_A=0.04$, and ϕ along path A in Fig. 2: liquid (left column) and glass (right column). The dashed line corresponds to the results at $\phi\simeq\phi_c\simeq 0.3782$. ϕ values for $\chi''_{10}(q,\omega)$ and $\chi''_{11}(q,\omega)$ are the same as for $\chi''_{00}(q,\omega)$.

time axis [73]. After a certain number of time steps the increment is doubled, etc. Although the t-dependent data shown in Fig. 5 look continuous, they exhibit tiny discontinuities of the correlators and of their first time derivatives at those times at which the increment is doubled. These discontinuities which could be diminished by an increase of the CPU time, lead to the wiggles which can be seen, e.g., in Fig. 6. However, we have checked by variation of the parameters h, the boundary values of the Fourier integrals, etc., that the features we will address below are not influenced by the wiggles. Further, the low frequency wing of the α-peak for $\chi''_{lm}(q,\omega)$ in Fig. 6 shows a rather small deviation from a linear ω-dependence, as it should. This failure is due to the choice of the lower bound for the Fourier integral. If this is taken to be zero, the wiggles become more pronounced. Therefore, choosing a nonzero bound is a compromise between reduction of the wiggles and a small deviation from linearity in ω for $\omega\to 0$. We have also used a spline technique for smoothing the data in time space. The Fourier transform of those data reproduced all the relevant features obtained from the original t-dependent correlators.

Let us now discuss the spectra. For $\phi<\phi_c(T^*_A)$, i.e., in the liquid phase, Fig. 6 left column reveals the existence of three peaks for $\chi''_{00}(q\simeq 4.7,\omega)$ and two peaks for $\chi''_{11}(q\simeq 4.7,\omega)$ and $\chi''_{10}(q\simeq 4.7,\omega)$. The low frequency peak in all spectra $\chi''_{lm}(q\simeq 4.7,\omega)$ is the α peak related to the slowing down of the structural relaxation (translational and rotational degrees of freedom). $\chi''_{00}(q\simeq 4.7,\omega)$ has a high frequency (hf) peak at $\omega_{hf}\approx 10$ and an additional peak at $\omega_{op}\simeq 1$, i.e., about one decade below the hf peak. $\chi''_{10}(q\simeq 4.7,\omega)$ and $\chi''_{11}(q\simeq 4.7,\omega)$ exhibit only one peak in the microscopic frequency domain at $\omega\approx\omega_{op}$. Below we will show that the peak in $\chi''_{00}(q\simeq 4.7,\omega)$ at $\omega\approx\omega_{op}$ originates from the orientational dynamics. Therefore we call it the ''orientational'' peak (subscript op).

The situation for $\phi>\phi_c(T^*_A)$, i.e., in the glass phase, is

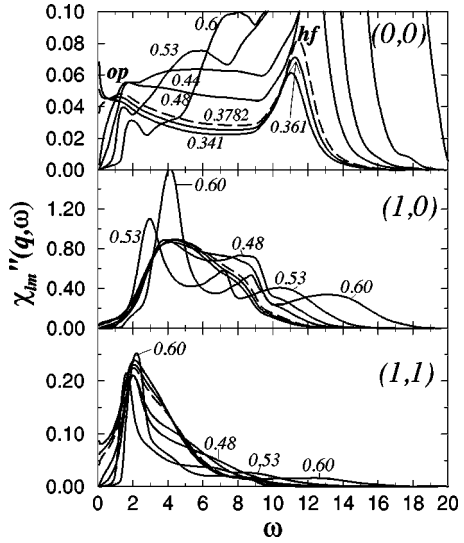

FIG. 7. $\chi''_{lm}(q,\omega)$ on linear scales at $q\simeq 4.7$, $T^*_A=0.04$, and ϕ along path *A* in Fig. 2. The dashed line corresponds to the results at $\phi\simeq\phi_c\simeq 0.3782$.

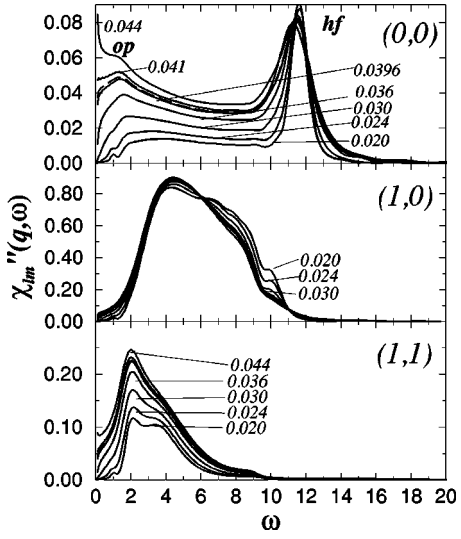

FIG. 8. $\chi''_{lm}(q,\omega)$ on linear scales at $q\simeq 4.7$, $\phi_C=0.3786$, and T^* along path *C* in Fig. 2. The dashed line corresponds to the result at $T^*\simeq T^*_c\simeq 0.04$.

similar with two exceptions (cf. right column of Fig. 6). First it is clear that there is no longer an α peak and second an additional peak located between the orientational and the hf peaks exists in $\chi''_{00}(q\simeq 4.7,\omega)$ for $\phi=0.53$ and 0.60, i.e., deep in the glass phase. A further ''peak'' looking more like a shoulder even appears for $\phi=0.6$. Such additional peaks can also be seen in $\chi''_{10}(q\simeq 4.7,\omega)$ and $\chi''_{11}(q\simeq 4.7,\omega)$ (cf. right column of Fig. 6).

In the following we will concentrate on the microscopic regime. Therefore we can use a linear ω scale, which allows us to recognize the ω and ϕ dependence (which we have described above) much better for $0.1<\omega<10$. This is done in Fig. 7 for the data from Fig. 6. Both microscopic peaks at $\omega_{op}\approx 1$ and $\omega_{hf}\approx 10$ can clearly be seen in the compressibility spectrum $\chi''_{00}(q\simeq 4.7,\omega)$. Whereas the intensity of the hf peak increases with increasing ϕ, the orientational peak becomes more pronounced when approaching the glass transition from the liquid side. In the glass phase at $\phi=0.44$ and $\phi=0.48$ it is less prominent but again becomes more pronounced for $\phi>0.5$, although its intensity decreases. The appearance of the intermediate peak for $\phi=0.53$ and $\phi=0.60$ at $\omega\approx 6$ and $\omega\approx 8$, respectively, can be observed, as well as the shoulder at $\omega\approx 4$. Due to the linear ω scale we clearly see that $\chi''_{10}(q\simeq 4.7,\omega)$ also exhibits an intermediate peak for $\phi=0.53$ and $\phi=0.60$, i.e., $\chi''_{10}(q\simeq 4.7,\omega)$ resembles $\chi''_{00}(q\simeq 4.7,\omega)$ but with the opposite ϕ dependence of the intensity of the orientational and hf peaks for $\phi>\phi_c(T^*_A)$. $\chi''_{11}(q\simeq 4.7,\omega)$, which is proportional to the dielectric loss $\epsilon''(q\simeq 4.7,\omega)$, possesses only one well pronounced peak at $\omega\approx\omega_{op}$. To check how far the features depend on the path through a critical point, we have investigated $\chi''_{lm}(q\simeq 4.7,\omega)$ along path *C* (see Fig. 1) for which $\phi=\phi_c=0.3786$ is fixed. This allows to study how far density and temperature variation lead to similar or different susceptibility spectra. The results for path *C* are given in Fig. 8. $\chi''_{00}(q\simeq 4.7,\omega)$ shows an orientational and a hf-peak at $\omega_{op}\approx 1$ and $\omega_{hf}\approx 10$, respectively. Their corresponding intensities behave qualitatively similarly for decreasing T^* as we found along path *A* for increasing ϕ. Intermediate peaks between the orientational and hf peaks do not occur. $\chi''_{10}(q\simeq 4.7,\omega)$ differs from the result along path *A*, whereas $\chi''_{11}(q\simeq 4.7,\omega)$ looks similar.

Translational and orientational dynamics freeze on paths *A* and *C* simultaneously. Therefore we have also calculated $\chi''_{lm}(q\simeq 4.7,\omega)$ on path *B* for fixed $T^*=0.30$ where $\phi_{00}(q,t)$ freezes at $\phi_c^{HS}\simeq 0.5265$ first, whereas $\phi_{lm}(q,t)$ undergoes a spin-glass-like transition at $\phi^c_{\text{type }A}(T^*=0.3)\simeq 0.62$. The corresponding results are presented in Fig. 9. $\chi''_{00}(q\simeq 4.7,\omega)$ and $\chi''_{lm}(q\simeq 4.7,\omega)$ exhibit a well pronounced main peak. Its po-

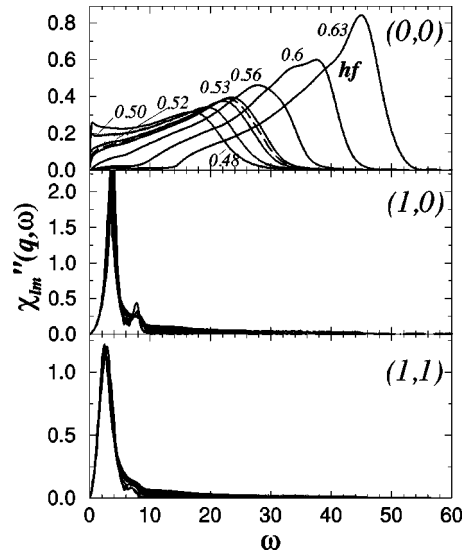

FIG. 9. $\chi''_{lm}(q,\omega)$ on linear scales at $q\simeq 4.7$, $T^*_B=0.3$, and ϕ along path *B* in Fig. 2. The dashed line corresponds to the result at $\phi\simeq\phi_c\simeq 0.5265$. Because $\chi''_{lm}(q,\omega)$ does not vary much with ϕ we have not labeled the various curves with ϕ.

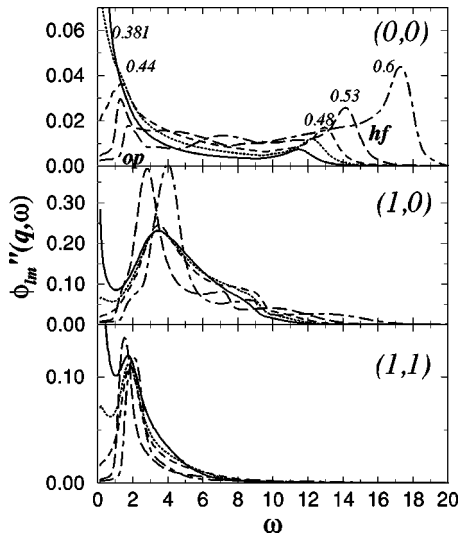

FIG. 10. $\phi''_{lm}(q\simeq 4.7,\omega)$ on linear scales in the glass phase along path *A* in Fig. 2, i.e., $T^*=0.04$ and $\phi=0.381$ (solid), $\phi=0.44$ (dotted), $\phi=0.48$ (dashed), $\phi=0.53$ (long-dashed), and $\phi=0.6$ (dot-dashed).

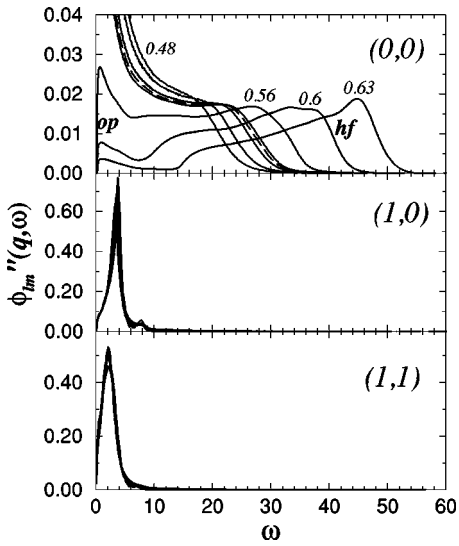

FIG. 11. $\phi''_{lm}(q\simeq 4.7,\omega)$ on linear scales for $T^*=0.30$ and ϕ along path *B* in Fig. 2. The dashed line corresponds to the result at $\phi\simeq\phi_c\simeq 0.5265$. Because $\phi''_{lm}(q,\omega)$ does not vary much with ϕ we have not labeled the various curves with ϕ.

sition depends sensitively on ϕ in the case of $\chi''_{00}(q\simeq 4.7,\omega)$ and is practically ϕ independent for $\chi''_{1m}(q\simeq 4.7,\omega)$. The latter quantity also posesses a small peak at $\omega\approx 10$, which originates from the translational motion via translation-rotation coupling.

A peak in the susceptibility spectra can be of either relaxational or oscillatory origin. To distinguish between the two types of behavior one must study the ω dependence of the correlation spectra $\phi''_{lm}(q,\omega)$. Spectra from neutron scattering are superpositions of $\phi''_{lm}(q,\omega)$ [65]. A peak in $\phi''_{lm}(q,\omega)$ at $\omega>0$ proves the existence of an oscillation whereas a peak at $\omega=0$ is of purely relaxational type. The corresponding peak width is a measure of the damping. These correlation spectra are shown in Figs. 10 and 11 for path *A* and path *B*, respectively. For $\phi<\phi_c(T^*)$ (not shown in Figs. 10 and 11) there is no peak at nonzero frequency, except for the hf peak. Therefore the orientational peak we found in $\chi''_{lm}(q\simeq 4.7,\omega)$ in the liquid phase is a purely relaxational excitation. Now let us discuss the correlation spectra in the glass phase. Figure 10 shows that in the glass, but close to the critical packing fraction, there is a hf peak at $\hat{\omega}_{hf}\approx 10$. Deeper in the glass the position of that hf peak shifts to higher frequencies and an orientational peak at $\hat{\omega}_{op}\approx 1$ appears. On decreasing ϕ even more an intermediate peak between the orientational and hf peaks is produced as well. The positions of the orientational and intermediate peaks shift to higher frequencies with decreasing ϕ like the hf peak, due to the increase of the glass stiffness. The ϕ dependence of $\phi''_{lm}(q\simeq 4.7,\omega)$ at much higher temperature $T^*=0.3$ (path *B* in Fig. 2) is presented in Fig. 11. We observe similar behavior as in Fig. 10, i.e., besides the hf peak at $\hat{\omega}_{hf}=20$–60 for $0.56\leqslant\phi\leqslant 0.63$ there occurs an orientational peak at $\hat{\omega}_{op}\approx 1$, and for $\phi=0.60$ and $\phi=0.63$ a shoulder at about $\omega\approx 20$ that corresponds to the intermediate peak in Fig. 10.

One of the conclusions we can draw from $\chi''_{lm}(q\simeq 4.7,\omega)$ and $\phi''_{lm}(q\simeq 4.7,\omega)$ is that there is an orientational peak at $\omega_{op}\approx\hat{\omega}_{op}\approx 1$ roughly one decade below the hf peak. The hf peak is related to a damped oscillation for the investigated range of T^* and ϕ, whereas the orientational peak changes its character from purely relaxational to damped oscillational behavior on going from the liquid to the glass. Since the dipolar spectra $\chi''_{lm}(q\simeq 4.7,\omega)$ and $\phi''_{lm}(q\simeq 4.7,\omega)$ have a main peak at about $\omega\approx 1$ it is tempting to associate the orientational peak in $\chi''_{00}(q\simeq 4.7,\omega)$ and $\phi''_{00}(q\simeq 4.7,\omega)$ with the orientational degrees of freedom and their coupling (via mode-coupling effects) to the translational ones. If this interpretation is correct then the orientational peak must exhibit an isotope effect with respect to a

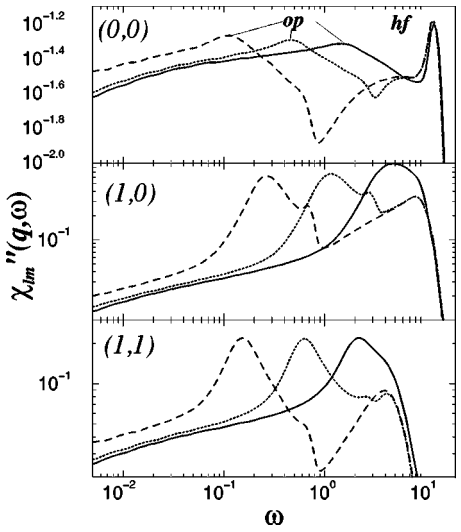

FIG. 12. $\chi''_{lm}(q\simeq 4.7,\omega)$ at $\phi=0.381$, $T^*=0.04$ for $I=\frac{1}{10}$ (solid), 1 (dotted), and 10 (dashed).

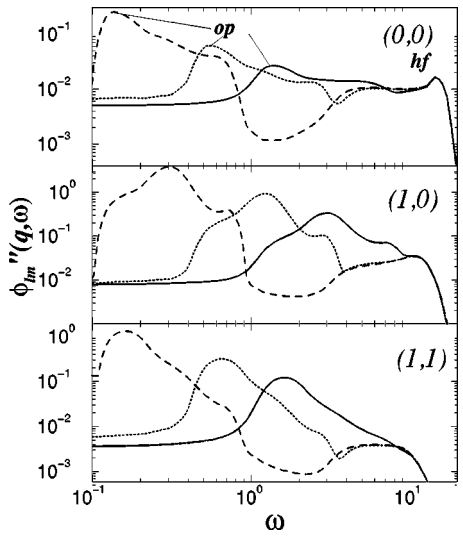

FIG. 13. $\phi_{lm}''(q\simeq 4.7,\omega)$ at $\phi=0.53$, $T^*=0.04$ for $I=\frac{1}{10}$ (solid), 1 (dotted), and 10 (dashed).

change of the moment of inertia I. Figure 12 presents $\chi_{lm}''(q\simeq 4.7,\omega)$ at $T_A^*=0.04$, $\phi=0.381$ for $I=1/10$ (the correct value for a hard sphere with $M=1$ and $d=1$ and homogeneous mass distribution), 1, and 10. From this result we find

$$\omega_{op}\propto\frac{1}{\sqrt{I}}. \tag{45}$$

This type of isotope effect also occurs for $\phi_{lm}''(q,\omega)$, which is shown in Fig. 13 for $\phi_{lm}''(q\simeq 4.7,\omega)$ at $T_A^*=0.04$, $\phi=0.530$, and for $I=1/10$, 1, and 10. This result yields:

$$\hat{\omega}_{op}\propto\frac{1}{\sqrt{I}}. \tag{46}$$

The approximate scaling of ω_{op} and $\hat{\omega}_{op}$ with $1/\sqrt{I}$ strongly supports the orientational origin of the orientational peak. Since ω_{hf} and $\hat{\omega}_{hf}$ are rather insensitive to a change of I their origin must lie in the translational motion.

So far we have not studied the q dependence of all of these peaks. Since this may further elucidate the features of the several peaks, we present $\chi_{lm}''(q,\omega)$ at $T_A^*=0.04$, $\phi=0.381$ in the glass but near the glass transition and $\phi_{lm}''(q,\omega)$ at $T_A^*=0.04$, $\phi=0.53$ deeper in the glass in Figs. 14 and 15, respectively. The result for $\chi_{00}''(q,\omega)$ shows a nearly q-independent position of the orientational peak at $\omega_{op}\approx 1$ for $1.0\leqslant q\leqslant 10.6$, whereas the position ω_{hf} of the hf peak changes with q. A similar q sensitivity holds for the position of the main microscopic peak in $\chi_{lm}''(q,\omega)$ for $m=0$ and 1. The result for $\phi_{lm}''(q,\omega)$ yields the same q independence of the orientational peak at $\hat{\omega}_{op}\simeq 1$ and a high sensitivity of the position of the hf peak at $\hat{\omega}_{hf}\approx 10$. The high frequency peak is essentially absent within a ''window'' around $q=6.5$ and appears below and above that window.

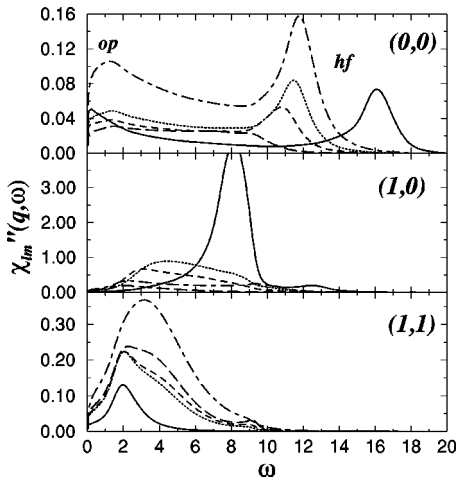

FIG. 14. q dependence of $\chi_{lm}''(q,\omega)$ at $\phi=0.381$, $T^*=0.04$ for $q\simeq 2.0$ (solid), $q\simeq 4.7$ (dotted), $q\simeq 5.3$ (dashed), $q\simeq 6.5$ (long-dashed), and $q\simeq 9.8$ (dot-dashed).

Finally, let us comment on the dependence of the peaks on T^* and ϕ as well as on α, which characterizes the distribution of the values for q [cf. Eq. (40) and Fig. 1]. Let us start with the α dependence. Figure 16 presents $\chi_{00}''(\overline{q_{max}},\omega)$ at $T_A^*=0.04$, $\phi=0.381$ for three different values of α. $\overline{q_{max}}$, which depends on α has been chosen as that q value closest to the main maximum of $S_{00}(q)$. Although the peak position and also the intensity vary with α the qualitative features do not depend on α, at least for reasonably chosen values of α.

The T^* dependence of the position ω_{op} and the height h_{op} of the orientational peak for $q\simeq 4.7$ is shown in Fig. 17(a) for $\phi_D=0.525$ along path D in Fig. 2. The corresponding ϕ dependence for the same q value and $T_A^*=0.04$ along path A is given in Fig. 17(b). h_{op} follows a linear T^* dependence between $T^*=0.04$ (the lowest temperature we have studied) and $T^*\approx 0.1$. In the temperature region where ω_{op}

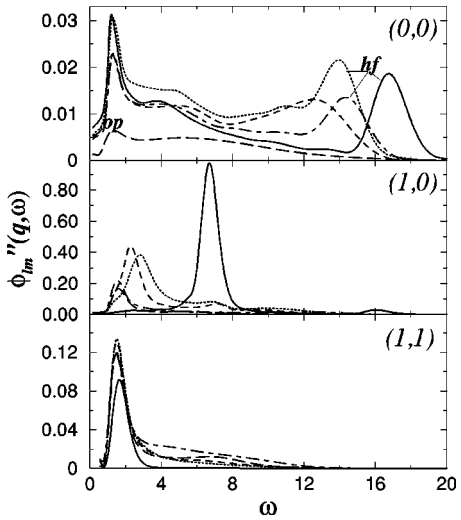

FIG. 15. q dependence of $\phi_{lm}''(q,\omega)$ at $\phi=0.53$, $T^*=0.04$ for $q\simeq 2.0$ (solid), $q\simeq 4.7$ (dotted), $q\simeq 5.3$ (dashed), $q\simeq 6.5$ (long-dashed), and $q\simeq 9.8$ (dot-dashed).

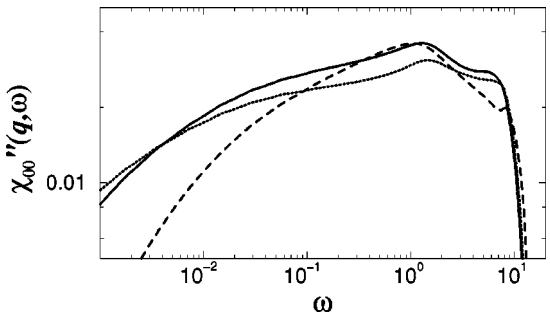

FIG. 16. α dependence of $\chi_{00}''(\bar{q}_{max},\omega)$ at $\phi=0.381$, $T^*=0.04$ for $\alpha=0.06$ (dashed), 0.065 (solid), and 0.068 (dotted).

has a minimum, h_{op} shows a crossover to a constant. As can be observed from Fig. 17b the position ω_{op} and the height h_{op} are almost constant below $\phi_c(T_A^*=0.04)\simeq 0.3782$ and increase with increasing ϕ above that value.

III. DISCUSSION AND CONCLUSIONS

Recently we extended the mode coupling theory for simple or binary liquids [1–4] to molecular liquids [6,7,68]. This was done within a molecular representation, which separates translational from orientational degrees of freedom. This molecular theory has already been applied and tested for diatomic molecules [77,12,13] and water molecules with the SPC/E potential [7,14]. These tests were restricted to a comparison of the nonergodicity parameters and critical amplitudes (for diatomic molecules only) from molecular MCT with the corresponding quantities from a MD simulation. A satisfactory agreement between MCT and MD simulation was found. So far no dynamical results have been determined from mode-coupling theory for *molecular liquids*. The only solution of the time-dependent MCT equations for a system with orientational degrees of freedom was obtained recently for the orientational correlators of a single dumbbell in an isotropic liquid [67,56]. In the present paper we have solved the time-dependent molecular MCT equations for a system of dipolar hard spheres. This is one of the simplest systems involving translational and orientational degrees of freedom. In addition, it has the advantage that the static correlators which are the input quantities for the MCT equations are known analytically within some approximations. These approximations make the tensorial correlators in the q frame $\phi_{lm,l'm'}(\vec{q}=\vec{q}_0,t)=\phi_{lm}(q,t)\delta_{ll'}\delta_{mm'}$ diagonal in l and l'. In addition they lead to a restriction of $\phi_{lm}(q,t)$ to $l=0,1$ only. This means that our calculations yield information on center of mass and dipolar dynamics.

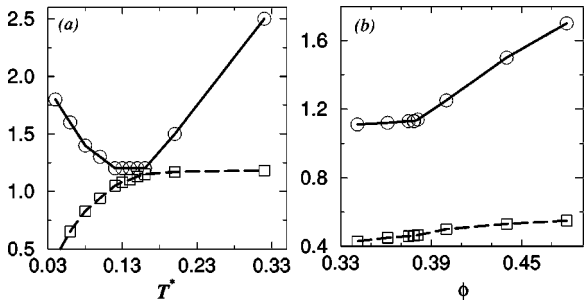

FIG. 17. (a) Temperature dependence of the position ω_{op} (○) and height h_{op} (□) (multiplied by 10) of the orientational peak for $q\simeq 4.7$ and $\phi_D=0.525$ along path D in Fig. 2. (b) Dependence on the packing fraction of the position ω_{op} (○) and height h_{op} (□) (multiplied by 10) of the orientational peak for $q\simeq 4.7$ and $T_A^*=0.04$ along path A in Fig. 2.

The major result we have found in the microscopic frequency regime is the existence of an orientational peak at $\omega_{op}(\text{liquid})\approx\hat{\omega}_{op}(\text{glass})$ about one decade below the high frequency peak. This orientational peak exists above and below the glass transition lines in the two dimensional phase diagram of dimensionless temperature T^* and packing fraction ϕ provided that the α-peak position ω_α is much smaller than ω_{op}. On the liquid side it exists in $\chi_{00}''(q,\omega)$, the compressibility spectrum, but not in $\phi_{00}''(q,\omega)$, which proves its pure relaxational character. However, on crossing the glass transition line this peak also appears in the correlation spectrum $\phi_{00}''(q,\omega)$ if T^* and ϕ become, respectively, small and large enough. This means that the orientational peak exists on *both* sides of the glass transition line and changes from a relaxational to a damped oscillational type of excitation under transformation of the liquid to the glass. The manner of development of the orientational peak in $\chi_{00}''(q,\omega)$ as a function of ϕ (see the double logarithmic representation in Fig. 6) resembles at least qualitatively the behavior of the extra peak in the susceptibility spectra for, e.g., salol and orthoterphenyl [78,20,79] at $\omega\approx 300$ GHz under variation of the temperature.

Since the position ω_{op} is almost independent of q it is related to a localized, nonpropagating mode. In addition, the isotope effect, i.e., $\omega_{op}\propto I^{-1/2}$, clearly proves its orientational origin. Since the bare frequencies $\Omega_{lm}(q)$ for $l=1$ scale with $I^{-1/2}$ for $q=0$ only [cf. Eq. (42)], the orientational peak must be generated by orientational modes with $q\approx 0$. Why do such long waved orientational modes play a crucial role? An answer follows from the static correlator $S_{11}(q)$. In contrast to $S_{00}(q)$ and $S_{10}(q)$ it exhibits a dominant peak with width Δq at $q=0$ and decays rapidly to 1 for $q>\Delta q$ (see Fig. 1). With decreasing temperature its peak height increases and Δq decreases. The increase of $S_{11}(q\approx 0)$ has two implications.

(i) Since the glass transition in MCT is driven by the increase of the main peaks of the static correlators,[1] it is the increase of $S_{11}(q\approx 0)$ and the coupling of the orientational mode $\rho_{11}(\vec{q},t)$ to $\rho_{00}(\vec{q},t)$, the translational one, that enhance the tendency for glass formation. This type of glass transition mechanism was already described within the framework of MCT for crystalline systems. For orientational glasses [84,85] and strictly periodic lattices [86,87] which undergo a second order equilibrium phase transition the in-

[1]That the underlying mechanism leading to an ideal glass transition can be much more sophisticated, i.e., not only related to the increase of, e.g., one peak in $S_{00}(q)$, has been recently demonstrated for a system of hard spheres with attractive interactions [80–83].

crease of the critical fluctuations already led to an ideal glass transition above the equilibrium transition temperature. The increase of the critical fluctuations is accompanied by softening of the critical mode.

(ii) Since $\Omega_{11}(q) \propto 1/\sqrt{S_{11}(q)}$ [cf. Eq. (42)] the increase of $S_{11}(q \approx 0)$ implies a softening of the orientational mode for $q \approx 0$ (see also Fig. 3). It is this softening of the orientational mode with $q \approx 0$ and $l=1$, $m=1$ that results in a frequency scale separation between this orientational mode and the translational one ($l=0$, $m=0$) with $q \approx q_{max}$. Therefore two peaks, the orientational and the hf peaks, become visible. The connection of $\hat{\omega}_{op}(q)$ with the (1,1) mode is also supported by the fact that $\hat{\omega}_{op}(q) \approx \hat{\Omega}_{11}^{\pm}(q)$ (see Fig. 4).

The narrowing of the peak in $S_{11}(q)$ at $q=0$ also has an interesting implication. Since $1/\Delta q$ is a measure of a correlation length, the narrowing implies growth of orientational order. Although $1/\Delta q$ does not diverge, it may be significantly larger than a few angstroms, i.e., there may exist a medium range orientational order. For instance, for $\phi = 0.381$ and $T^* = 0.04$ the correlation length is about six diameters (cf. Fig. 1). The fact that the increase of $S_{11}(q \approx 0)$ is accompanied by narrowing of the peak in $S_{11}(q)$ at $q=0$ proves the existence of a correlation between the occurrence of the orientational peak and medium range orientational order. This is an interesting observation insofar as such a correlation has already been predicted [88–90,39,91], although this does not seem to be a universal feature [92]. We emphasize that we do not consider this type of behavior as an exceptional case which exists for dipolar hard spheres only. For example for a system of hard ellipsoids which may exhibit medium ranged nematic order (see Ref. [93]) similar results are expected.

That a soft mode will lead to an additional microscopic peak in the spectra has already been shown [94] for a so-called schematic model [1]. Qualitative features of the static and dynamical behavior of dipolar hard spheres can also be described by a schematic model. Details will be given elsewhere. The couplings shown in Eqs. (38) and (39) suggest the use of two correlators $\phi_0(t)$ and $\phi_1(t)$, only. $\phi_0(t)$ and $\phi_1(t)$ corresponds to the center of mass and the dipolar correlators, respectively, and their dynamics is described by the Bosse-Krieger model [95]:

$$\ddot{\phi}_a(t) + \Omega_a^2 \phi_a(t) + \nu_a \dot{\phi}_a(t) + \Omega_a^2 \int_0^t dt' m_a(t-t') \dot{\phi}_a(t') = 0, \tag{47}$$

$a=0,1$, with the memory kernels

$$m_0(t) \equiv F_0(\phi_0(t), \phi_1(t)) = \xi_1 \phi_0^2(t) + \xi_2 \phi_1^2(t), \tag{48a}$$

$$m_1(t) \equiv F_1(\phi_0(t), \phi_1(t)) = \xi_3 \phi_0(t) \phi_1(t), \tag{48b}$$

and initial conditions $\phi_a(0)=1$, $\dot{\phi}_a(t)=0$. To mimic the ϕ and T dependence of the dipolar hard spheres we choose

$$\xi_1 \equiv \phi, \quad \xi_2 \equiv x/T, \quad \xi_3 \equiv 1/T. \tag{49}$$

In Fig. 18 we present $\phi_0(t)$ for fixed frequency $\Omega_0=1$

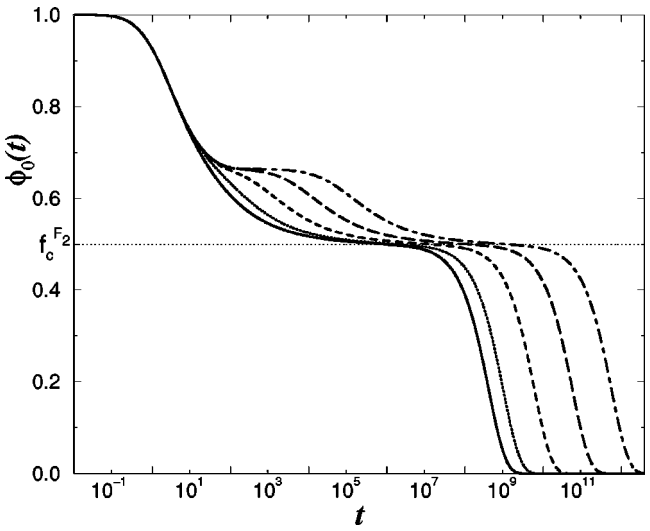

FIG. 18. $\phi_0(t)$ for the Bosse-Krieger model for $T=0.7$, $\phi = 3.9995$, $x=0.15$, $\Omega_0=1$, $\nu_0=10$, $\nu_1=1$, and different $\Omega_1 = 10^{-n/2}$, $n=0,1,2,3,4$ from left to right. f_c^{F2} denotes the critical nonergodicity parameter of the F_2 model.

and different values of Ω_1. For $\Omega_1=\Omega_0$ we find the typical two step relaxation process from $\phi_0(0)=1$ to a plateau at $f_c \equiv f_c^{F_2}$ and a final decay to zero. With decreasing Ω_1 we observe that a shoulder occurs which finally develops into a second plateau above $f_c^{F_2}$. This can easily be understood. In case that Ω_1 becomes more and more soft with respect to Ω_0, the second term in $m_0(t)$ [cf. Eq. (48a)] already varies more and more slowly on the microscopic time scale $t_0 = \Omega_0^{-1}$. Therefore the relaxation kernel $m_0(t)$ has a rather slowly varying part. It is this part that generates the second plateau. Since the decay from a pronounced plateau produces a relaxation peak in the corresponding susceptibility spectrum we expect, besides the high frequency peak related to Ω_0 and the α peak, one more peak. This peak stems from the decay from the upper plateau to that at $f_c^{F_2}$.

Figure 19, which shows $\chi_a''(\omega)$ at rather ''low'' tempera-

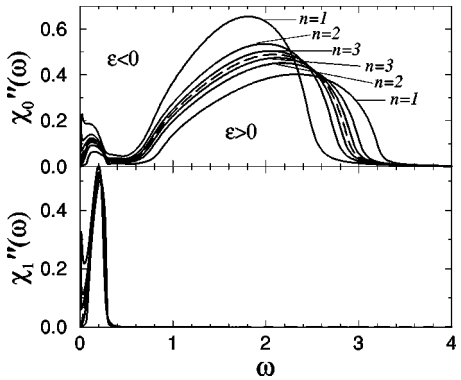

FIG. 19. $\chi_a''(\omega)$ for $\Omega_0=1$, $\Omega_1=1/10$, $\nu_0=\nu_1=0$, $x=0.15$, and $T=0.2$ along path A in Fig. 2 for $\phi=(1+\varepsilon)\phi_c$, $\phi_c \simeq 2.893\,131\,8$, $\varepsilon = \pm e^{-n}$, $n=1,2,3$ (solid lines), and $\phi=\phi_c$ (dashed line). Because $\chi_1''(\omega)$ does not vary much with ϕ we have not labeled the various curves with n.

tures, confirms this observation. There is an additional microscopic peak at $\omega \approx \Omega_1$, i.e., at about the frequency of the ''soft mode.'' Investigating $\phi_a''(\omega)$, we have found that this additional peak does not occur in the liquid phase but deeper in the glass. Therefore, the nature of that peak changes from relaxational in the ergodic phase to underdamped oscillational in the nonergodic phase, quite like the orientational peak for dipolar hard spheres.

Besides the orientational peak, we have found in $\chi_{00}''(q,\omega)$ and $\phi_{00}''(q,\omega)$ above and below the glass transition a high frequency peak at $\omega_{hf}(q)$. It exists in the investigated range $0.51 < q < 40$ except in an interval centered around q_{max}, the position of the main peak in $S_{00}(q)$. $\omega_{hf}(q)$ is shown in Fig. 4 for $q \leqslant 2$. Despite an inaccuracy of about 10 (due to the q discretization) its q dependence is in phase with the q variation of the renormalized frequency $\hat{\Omega}_{00}(q)$. These qualitative features are similar to those of the type of high frequency peak found for a system of hard spheres [57]. Since the accuracy of $\omega_{hf}(q)$ becomes even worse for $q \rightarrow 0$ it is not possible to detect the expected linear q dependence for $q \rightarrow 0$. Accordingly, we cannot yet prove that the hf peak for dipolar hard spheres corresponds to high frequency sound, as found for the system of hard spheres [57]. In [57] it was also shown that an additional peak, which was called the anomalous oscillation peak, appears deep in the glass phase. Its origin lies in the harmonic motion of the particles in their cages [57]. Whether or not the hump between the orientational peak and the hf peaks that we observed in $\phi_{00}''(q,\omega)$ deep in the glass (see Figs. 10 and 15) corresponds to the AOP is not clear. Again, due to the restriction to 30 values for q and also a smaller number of discrete values for t compared to Ref. [57] we cannot give detailed *quantitative* information on, e.g., the q dependence of the position and width of that hump. On the other hand, the high frequency wing of the orientational peak may interfere with the AOP, thus complicating the analysis of the latter.

A well-pronounced two peak structure in the microscopic frequency regime can also occur for $\chi_{10}''(q,\omega)$ (cf. Fig. 7) deep in the glass, whereas this does not happen for $\chi_{11}''(q,\omega)$ (cf. Fig. 7) which is directly related to the dielectric loss spectrum $\epsilon''(q,\omega)$.

Let us come back to the orientational peak. Figure 17(a) shows that its intensity varies linearly with temperature below about $T^* = 0.13$ and for $\phi_D = 0.525$, i.e., for T^* smaller than $T_c^*(\phi_D = 0.525) \simeq 0.13$. This fact, as well as the the lack of sensitivity of its position ω_{op} to q and its location about one decade below the high frequency peak, is reminiscent of the boson peak. Additionally, the increase of ω_{op} with increasing packing fraction is similar to the shift of the boson peak to higher frequency on increasing the pressure [96–98].

To conclude, we can say that we have found in the microscopic frequency regime of the compressibility spectrum and the corresponding correlation spectrum an additional orientational low frequency peak. It originates from a localized and nonpropagating orientational mode coupled to longitudinal acoustic sound waves (translational modes). Its dynamical origin changes from a pure relaxational to a damped oscillational type when crossing the glass transition from the liquid side. Since the orientational frequency has a gap at $q = 0$ the orientational excitation is an optical mode. These characteristic features coincide with several explanations for the existence of the boson peak [18,35,58,62,63], which may stress the role of orientational degrees of freedom. It is also interesting that the intensity of the orientational peak in a certain temperature regime [cf. Fig. 17(a)] changes linearly with T^*, which is also true for the boson peak. In addition, we have found an interesting correlation between the orientational peak phenomenon and a medium range orientational order, as already suggested earlier for the boson peak [88–90,39,91], although it has been shown that this does not seem to hold for all glass formers [92].

For dipolar hard spheres this order is of ferroelectric type and for hard ellipsoids it is related to a precursor of nematic order. For SiO_2 it can occur due to strong orientational bond interactions. As demonstrated in the present paper this medium range orientational order may result in softening of a localized, optic orientational mode and may finally generate an additional microscopic peak about one decade below the high frequency peak.

In general, it is not easy to separate the contribution from the orientational motion from experimental spectra obtained from light or neutron scattering. But this is not true for a MD simulation. Due to the availability of all the microscopic information it would be desirable to explore in more detail by MD simulations the role of the orientational degrees of freedom in the glass transition itself and also in the spectra in the microscopic regime, as has already been done for sound propagation in liquid water [99].

Finally, we mention that the microscopic spectral features we have found for dipolar hard spheres can be qualitatively reproduced by use of a schematic model, the Bosse-Krieger model.

ACKNOWLEDGMENTS

We are grateful to W. Götze for his careful reading of this manuscript and many valuable comments, to M. Sperl and Th. Voigtmann for their discussion with respect to the accuracy of our numerical results, and to P. A. Madden for the discussion on orientational modes in molecular liquids. Financial support by Sonderforschungsbereich 262 is also gratefully acknowledged.

APPENDIX: THE NUMERICALLY SOLVED MCT EQUATIONS

Using the continuity equation we get the first equation of motion for the generalized density-density correlation functions (in the q frame):

$$\dot{S}_{ll'm}(q,t) = -i \sum_{\alpha = R,T} q_l^{\alpha}(q)\, \phi_{ll'm}^{j^{\alpha}\rho}(q,t) \qquad \text{(A1)}$$

with

$$\phi^{j^\alpha\rho}_{ll'm}(q,t) := \frac{1}{N}\langle j^{\alpha *}_{lm}(q,t)\rho_{l'm'}(q,0)\rangle \delta_{mm'} \tag{A2}$$

the *density–current-density correlation function*. Projecting on the tensorial densities [6] and the longitudinal translational and rotational current densities [6] in one step leads to

$$\begin{aligned}\dot{\phi}^{j^\alpha\rho}_{ll'm}(q,t) = &-i\sum_{l_2=0}^{l_{co}-m} q^\alpha_l(q)\frac{k_BT}{I_\alpha}(\mathbf{S}^{-1}(q))_{ll_2m}S_{l_2l'm}(q,t)\\ &-\sum_{l_2=0}^{l_{co}-m}\sum_{\alpha'=R,T}\frac{k_BT}{I_\alpha}\int_0^t dt' M^{\alpha\alpha'}_{ll_2m}(q,t-t')\\ &\times\phi^{j^{\alpha'}\rho}_{l_2l'm}(q,t')\end{aligned} \tag{A3}$$

with the cutoff value l_{co} for l [for dipolar hard spheres it is $l_{co}=1$; cf. Eqs. (36) and (37)] and I_α defined in Eq. (9). To make use of the established numerical method to solve such equations [73], it is necessary to introduce auxiliary functions Φ:

$$\dot{\Phi}^{j^\alpha\rho}_{ll'm}(q,t) := q^\alpha_l(q)\phi^{j^\alpha\rho}_{ll'm}(q,t). \tag{A4}$$

As a consequence Eq. (A1) reduces to

$$S_{ll'm}(q,t) = -i\sum_{\alpha=R,T}\Phi^{j^\alpha\rho}_{ll'm}(q,t) \tag{A5}$$

where $\Phi^{j^\alpha\rho}_{ll'm}(q,t)$ is determined only up to an integration constant which does not influence the result for $S_{ll'm}(q,t)$. Making use of Eq. (A4) and taking the time derivative of Eq. (A3) leads to a set of equations of similar structure to the MCT equations for simple liquids [1,2,4,3]. The molecular MCT equations do not couple only all (*discretized*) wave vectors, as in simple liquids, but also the indices $\alpha=T,R$ for translation and rotation and the spherical indices $l\leqslant l_{co}$ and $-l\leqslant m\leqslant l$. The functions Φ are auxiliary functions because their introduction is just for numerical purposes. The integral in Eq. (A3) transforms to

$$\int_0^t dt' M^{\alpha\alpha'}_{ll_2m}(q,t-t')\dot{\Phi}^{j^{\alpha'}\rho}_{l_2l'm}(q,t'). \tag{A6}$$

Now a time derivative is multiplied by the integration measure dt. As a consequence the time step Δt cancels in a discretized form of Eq. (A6). Using the decimation technique [73] Δt becomes very large. In this case the calculation of the integrals would become unstable if Δt did not cancel.

Since the auxiliary functions occur only as time derivatives in the original equations the result is independent of the initial values of $\Phi^{j^\alpha\rho}_{ll'm}(q,t=0)$. When solving the molecular MCT equations we have chosen

$$\Phi^{j^T\rho}_{0l'm}(q,t=0) = S_{0l'm}(q), \tag{A7a}$$

$$\Phi^{j^R\rho}_{0l'm}(q,t=0) = 0 \tag{A7b}$$

for all l' and

$$\Phi^{j^T\rho}_{ll'm}(q,t=0) = \frac{1}{2}S_{ll'm}(q), \tag{A7c}$$

$$\Phi^{j^R\rho}_{ll'm}(q,t=0) = \frac{1}{2}S_{ll'm}(q) \tag{A7d}$$

for $l>0$ as initial values.

[1] W. Götze, in, *Liquids, Freezing and the Glass Transition*, edited by J. P. Hansen, D. Levesque, and J. Zinn-Justin (North-Holland, Amsterdam, 1991).
[2] W. Götze and L. Sjögren, Rep. Prog. Phys. **55**, 241 (1992).
[3] R. Schilling, *Disorder Effects on Relaxation Processes*, edited by R. Richter and A. Blumen (Springer, Berlin, 1994).
[4] H. Z. Cummins, J. Phys.: Condens. Matter **11**, A95 (1999).
[5] T. Franosch, M. Fuchs, W. Götze, M. R. Mayr, and A. P. Singh, Phys. Rev. E **56**, 5659 (1997).
[6] R. Schilling and T. Scheidsteger, Phys. Rev. E **56**, 2932 (1997).
[7] L. Fabbian, A. Latz, R. Schilling, F. Sciortino, P. Tartaglia, and C. Theis, Phys. Rev. E **60**, 5768 (1999).
[8] Transp. Theory Stat. Phys. **24**, 6 (1995), special issue on relaxation kinetics in supercooled liquids–mode-coupling theory and its experimental tests, edited by S. Yip.
[9] W. Kob, J. Phys.: Condens. Matter **11**, R85 (1999).
[10] W. Götze, J. Phys.: Condens. Matter **11**, A1 (1999).
[11] N. Tao, G. Li, X. Chen, W. Du, and H. Z. Cummins, Phys. Rev. A **44**, 6665 (1991).
[12] R. Schilling, J. Phys.: Condens. Matter **12**, 6311 (2000).
[13] A. Winkler, A. Latz, R. Schilling, and C. Theis, Phys. Rev. E **62**, 8004 (2000).
[14] C. Theis, F. Sciortino, A. Latz, R. Schilling, and P. Tartaglia, Phys. Rev. E **62**, 1856 (2000).
[15] C. Theis and R. Schilling, J. Non-Cryst. Solids **235-237**, 106 (1998).
[16] R. O. Pohl, *Amorphous Solids—Low Temperature Properties*, *Topics in Current Physics*, edited by W. A. Phillips (Springer, Berlin, 1981).
[17] V. K. Malinovski and A. P. Sokolov, Solid State Commun. **57**, 757 (1986).
[18] U. Buchenau, N. Nücker, and A. J. Dianoux, Phys. Rev. Lett. **53**, 2316 (1984).
[19] U. Buchenau, M. Prager, N. Nücker, A. J. Dianoux, N. Ahmad, and W. A. Phillips, Phys. Rev. B **34**, 5665 (1986).
[20] H. Z. Cummins, G. Li, W. Du, Y. H. Hwang, and G. Q. Shen, Prog. Theor. Phys. Suppl. **26**, 21 (1997).
[21] M. C. C. Ribeiro, M. Wilson, and P. A. Madden, J. Chem. Phys. **109**, 9859 (1998); **110**, 4803 (1999).
[22] P. Benassi, M. Krisch, C. Masciovecchio, V. Mazzacurati, G. Monaco, G. Ruocco, F. Sette, and R. Verbeni, Phys. Rev. Lett. **77**, 3835 (1996).

[23] M. Foret, E. Courtens, R. Vacher, and J.-B. Suck, Phys. Rev. Lett. **77**, 3831 (1996).
[24] M. Foret, E. Courtens, R. Vacher, and J.-B. Suck, Phys. Rev. Lett. **78**, 4669 (1997).
[25] P. Benassi, M. Krisch, C. Masciovecchio, V. Mazzacurati, G. Monaco, G. Ruocco, F. Sette, and R. Verbeni, Phys. Rev. Lett. **78**, 4670 (1997).
[26] A. Matic, L. Börjesson, G. Ruocco, C. Masciovecchio, A. Mermet, F. Sette, and R. Verbeni, Europhys. Lett. **54**, 77 (2001).
[27] C. Masciovecchio, A. Mermet, G. Ruocco, and F. Sette, Phys. Rev. Lett. **85**, 1266 (2000).
[28] O. Pilla, A. Cunsolo, A. Fontana, C. Masciovecchio, G. Monaco, M. Montagna, G. Ruocco, T. Scopigno, and F. Sette, Phys. Rev. Lett. **85**, 2136 (2000).
[29] J. Horbach, W. Kob, and K. Binder, in *Neutrons and Numerical Methods–N_2M*, edited by M. R. Johnson *et al.* AIP Conf. Proc. 479 (AIP, Woodbury, NY, 1999), p. 136.
[30] J. Horbach, W. Kob, and K. Binder, Eur. Phys. J. B **19**, 531 (2001).
[31] C. Masciovecchio, G. Ruocco, F. Sette, M. Krisch, R. Verbeni, U. Bergmann, and M. Soltwisch, Phys. Rev. Lett. **76**, 3356 (1996).
[32] M. Sampoli, G. Ruocco, and F. Sette, Phys. Rev. Lett. **79**, 1678 (1997).
[33] H. R. Schober and C. Oligschleger, Phys. Rev. B **53**, 11 469 (1996).
[34] S. N. Taraskin and S. R. Elliott, Europhys. Lett. **39**, 37 (1997).
[35] S. N. Taraskin and S. R. Elliott, Phys. Rev. B **56**, 8605 (1997).
[36] S. N. Taraskin and S. R. Elliott, Phys. Rev. B **59**, 8572 (1999).
[37] S. N. Taraskin and S. R. Elliott, J. Phys.: Condens. Matter **11**, A219 (1999).
[38] V. Mazzacurati, G. Ruocco, and M. Sampoli, Europhys. Lett. **34**, 681 (1996).
[39] M. Foley, M. Wilson, and P. A. Madden, Philos. Mag. B **71**, 557 (1995).
[40] M. C. C. Ribeiro, M. Wilson, and P. A. Madden, J. Chem. Phys. **108**, 9027 (1999).
[41] D. Engberg, A. Wischnewski, U. Buchenau, L. Börjeson, A. J. Dianoux, A. P. Sokolov, and L. M. Torell, Phys. Rev. B **58**, 9087 (1998).
[42] A. P. Sokolov, J. Phys.: Condens. Matter **11**, A213 (1999).
[43] W. Schirmacher and M. Wagner, in *Dynamics of Disordered Materials*, edited by D. Richter, A. J. Dianoux, W. Petry, and J. Teixeira (Springer, Berlin, 1989), pp. 231–234.
[44] W. Schirmacher, G. Diezemann, and C. Ganter, Phys. Rev. Lett. **81**, 136 (1998).
[45] V. Martín-Mayor, G. Parisi, and P. Verrocchio, Phys. Rev. E **62**, 2373 (2000).
[46] M. Mézard, G. Parisi, and A. Zee, e-print cond-mat/9906135.
[47] V. G. Karpov, M. I. Klinger, and F. N. Ignat'ev, Sov. Phys. JETP **57**, 439 (1983).
[48] M. I. Klinger, Phys. Rep. **165**, 275 (1988).
[49] Yu. M. Galperin, V. L. Gurevich, and D. A. Parshin, Phys. Rev. B **32**, 6873 (1992).
[50] U. Buchenau, Yu. M. Galperin, V. L. Gurevich, D. A. Parshin, M. A. Ramos, and H. R. Schober, Phys. Rev. B **46**, 2798 (1992).
[51] C. Alba-Simionesco and M. Krauzman, J. Chem. Phys. **102**, 6574 (1995).
[52] W. Götze and L. Sjögren, Chem. Phys. **212**, 47 (1996).
[53] T. Franosch, W. Götze, M. R. Mayr, and A. P. Singh, Phys. Rev. E **55**, 3183 (1997).
[54] S. P. Das, Phys. Rev. E **59**, 3870 (1999).
[55] B. Ruffle, C. Ecolivet, and B. Toudic, Europhys. Lett. **45**, 591 (1999).
[56] W. Götze and T. Voigtmann, Phys. Rev. E **61**, 4133 (2000).
[57] W. Götze and M. R. Mayr, Phys. Rev. E **61**, 587 (2000).
[58] B. Guillot and Y. Guissani, Phys. Rev. Lett. **78**, 2401 (1997).
[59] A. Wischnewski, U. Buchenau, A. J. Dianoux, W. A. Kamitakahara, and J. L. Zarestky, Phys. Rev. B **57**, 2663 (1998).
[60] U. Schneider, P. Lunkenheimer, R. Brand, and A. Loidl, Phys. Rev. E **59**, 6924 (1999).
[61] P. Lunkenheimer, R. Brand, U. Schneider, and A. Loidl, Contemp. Phys. **41**, 15 (2000).
[62] M. A. Ramos, S. Viera, F. J. Bermejo, J. Dawidowski, H. E. Fischer, H. Schober, M. A. Gonzalez, C. K. Loong, and D. L. Price, Phys. Rev. Lett. **78**, 82 (1997).
[63] H. E. Fischer, E. J. Bermejo, G. J. Cuello, M. T. Fernandez-Diaz, J. Davidowski, M. A. Gonzalez, H. Schober, and H. Jimenez-Ruiz, Phys. Rev. Lett. **82**, 1193 (1999).
[64] J. P. Hansen and I. R. McDonald, *Theory of Simple Liquids*, 2nd ed. (Academic Press, London, 1986).
[65] C. Theis and R. Schilling, Phys. Rev. E **60**, 740 (1999).
[66] S.-H. Chong and F. Hirata, Phys. Rev. E **58**, 6188 (1998).
[67] S.-H. Chong, W. Götze, and A. P. Singh, Phys. Rev. E **63**, 011 206 (2000).
[68] A. Latz and M. Letz, Eur. J. Phys. **19**, 3239 (2001).
[69] M. A. Ricci, D. Rocca, G. Ruocco, and R. Vallauri, Phys. Rev. A **40**, 7226 (1989).
[70] M. S. Wertheim, J. Chem. Phys. **55**, 4291 (1971).
[71] C. G. Gray and K. E. Gubbins, *Theory of Molecular Liquids* (Clarendon, Oxford, 1984).
[72] A. Latz, Ph.D. thesis, Technische Universität München, 1990.
[73] M. Fuchs, W. Götze, I. Hofacker, and A. Latz, J. Phys.: Condens. Matter **3**, 5047 (1991).
[74] W. Götze, A. P. Singh, and T. Voigtmann, Phys. Rev. E **61**, 6934 (2000).
[75] T. Scheidsteger and R. Schilling, Philos. Mag. B **77**, 305 (1998).
[76] T. Franosch, M. Fuchs, W. Götze, M. R. Mayr, and A. P. Singh, Phys. Rev. E **55**, 7153 (1997).
[77] C. Theis and R. Schilling, J. Non-Cryst. Solids **235-237**, 106 (1998).
[78] H. Z. Cummins, W. M. Du, M. Fuchs, W. Götze, S. Hildebrand, A. Latz, G. Li, and N. J. Tao, Phys. Rev. E **47**, 4223 (1993).
[79] H. Z. Cummins, Y. H. Hwang, Gen Li, W. M. Du, W. Losert, and G. Q. Shen, J. Non-Cryst. Solids **235-237**, 254 (1998).
[80] L. Fabbian, W. Götze, F. Sciortino, P. Tartaglia, and F. Thiery, Phys. Rev. E **59**, R1347 (1999).
[81] E. Zaccarelli, G. Foffi, K. A. Dawson, F. Sciortino, and P. Tartaglia, Phys. Rev. E **63**, 031501 (2001).
[82] K. Dawson, G. Foffi, M. Fuchs, W. Götze, F. Sciortino, M. Sperl, P. Tartaglia, T. Voigtmann, and E. Zaccarelli, Phys. Rev. E **63**, 011140 (2001).

[83] J. Bergenholtz and M. Fuchs, Phys. Rev. E **59**, 5706 (1999).
[84] K. H. Michel, Z. Phys. B: Condens. Matter **71**, 369 (1988).
[85] C. Bostoen and K. H. Michel, Phys. Rev. B **43**, 4415 (1991).
[86] V. L. Aksenov, M. Bobeth, N. M. Plakida, and J. Schreiber, J. Phys. C **20**, 375 (1987).
[87] R. Schilling, Z. Phys. B: Condens. Matter **103**, 463 (1997).
[88] S. R. Elliott, Phys. Rev. Lett. **67**, 711 (1991).
[89] A. P. Sokolov, A. Kisliuk, M. Soltwisch, and D. Quitmann, Phys. Rev. Lett. **69**, 1540 (1992).
[90] A. P. Sokolov, A. Kisliuk, M. Soltwisch, and D. Quitmann, Physica A **201**, 295 (1993).
[91] R. Fayos, F. J. Bermejo, J. Dawidowski, H. E. Fischer, and M. A. Gonzales, Phys. Rev. Lett. **77**, 3823 (1996).
[92] L. Börjesson, A. K. Hassan, J. Swenson, and L. M. Torell, Phys. Rev. Lett. **70**, 1275 (1993).
[93] M. Letz, R. Schilling, and A. Latz, Phys. Rev. E **62**, 5173 (2000).
[94] T. Franosch, W. Götze, M. R. Mayr, and A. P. Singh, J. Non-Cryst. Solids **235-237**, 71 (1998).
[95] U. Krieger and J. Bosse, J. Phys. C **19**, L609 (1986).
[96] S. Sugai and A. Onodera, Phys. Rev. Lett. **77**, 4210 (1996).
[97] Y. Inamura, M. Arai, O. Yamamuro, A. Inaba, N. Kitamura, T. Otomo, T. Matsua, S. M. Bennington, and A. C. Hannon, Physica B **263**, 299 (1999).
[98] P. Jund and R. Jullien, J. Chem. Phys. **113**, 2768 (2000).
[99] F. Sciortino and S. Sastry, J. Chem. Phys. **100**, 3881 (1994).